Key factors affecting the stability of $CsPbI_3$ perovskite quantum dot solar cells: a comprehensive review

Seyeong Lim,‡ Sanghun Han,‡ Dohyun Kim, Jihyun Min, Jongmin Choi and Taiho Park**

S. Lim, D. Kim, J. Min, Prof. T. Park

Department of Chemical Engineering, Pohang University of Science and Technology (POSTECH), Pohang, Gyeongbuk 37673, Republic of Korea.

E-mail: taihopark@postech.ac.kr

S. Han, Prof. J. Choi

Department of Energy Science and Engineering, Daegu Gyeongbuk Institute of Science and Technology (DGIST), Daegu 42988, Republic of Korea.

E-mail: whdals1062@dgist.ac.kr

This article has been accepted for publication and undergone full peer review but has not been through the copyediting, typesetting, pagination and proofreading process, which may lead to differences between this version and the Version of Record. Please cite this article as doi: 10.1002/adma.202203430.

Keywords: $CsPbI_3$ perovskite quantum dots; solar cells; phase stability; environmental stability; device stability

Abstract

The power conversion efficiency of $CsPbI_3$ perovskite quantum dot (PQD) solar cells has increased from 10.77% to 16.2% in a short period owing to advances in material and device design for solar cells. However, the device stability of $CsPbI_3$ PQD solar cells remained poor in ambient conditions, which requires an in-depth understanding of the degradation mechanisms of $CsPbI_3$ PQDs solar cells in terms of both inherent material properties and device characteristics. Along with this analysis, advanced strategies to overcome poor device stability must be conceived. In this review, fundamental mechanisms that cause the degradation of $CsPbI_3$ PQD solar cells are discussed from the material property and device viewpoints. In addition, based on detailed insights into degradation mechanisms in $CsPbI_3$ PQD solar cells, various strategies are introduced to improve the stability of $CsPbI_3$ PQD solar cells. Finally, future perspectives and challenges are presented to achieve highly durable $CsPbI_3$ PQD solar cells. The investigation of the degradation mechanisms and the stability enhancement strategies can pave the way for the commercialization of $CsPbI_3$ PQD solar cells.

1. Introduction

Organic–inorganic lead halide perovskites (LHPs) have been widely used as photoactive materials for optoelectronic applications[1-3] (e.g., solar cells, light-emitting diodes, and photodetectors) owing to their high absorption coefficient, low exciton binding energy, high charge carrier mobility, and high defect tolerance.[4-7] With these outstanding properties and developments in the processing of materials and devices, organic–inorganic LHP solar cells showed rapid growth and remarkable performance in the last decades.[1, 8-11] The photovoltaic performance of organic–inorganic LHP solar cells increased up to a power conversion efficiency (PCE) of 25.7%.[12] However, their low stability under environmental stress has been considered a major obstacle to their commercialization.[13]

Organic–inorganic LHPs with an $APbI_3$ structure are easily decomposed into PbI_2 and other organic compounds due to volatile organic A-site cations, such as methylammonium (MA) and formamidinium (FA).[14,15] To address this issue, several strategies have been proposed, such as grain boundary passivation and the introduction of large organic cations into the A-site.[16] Meanwhile, replacing organic cations with robust inorganic cations can enhance thermal stability. From this point of view, all-inorganic perovskites without volatile organic components have attracted interest as

alternative materials to organic–inorganic LHPs.[17,18] In particular, all-inorganic $CsPbI_3$ perovskites are promising materials for solar cell applications, demonstrating charge carrier mobilities comparable to those of organic–inorganic LHPs, a bandgap of 1.73 eV, and a PCE over 20%.[19]

Despite the impressive thermal stability of all-inorganic LHPs, they undergo thermodynamic phase transition under device operation conditions. Unfortunately, photoactive cubic $CsPbI_3$ perovskites are easily converted to the photoinactive orthorhombic phase at room temperature (RT) because they are stable at temperatures above 300 °C.[17,20] Due to this thermodynamic phase instability, it is challenging to fabricate stable cubic $CsPbI_3$ perovskite films at RT. To address this issue, in 2015, Kovalenko *et al.* reduced the crystal size of $CsPbI_3$ perovskites to the nanoscale.[21] Crystal size and surface energy affect phase stability, and it was demonstrated that the crystal size reduced to the nanoscale can enhance the contribution of surface energy, stabilizing the cubic phase of $CsPbI_3$ perovskites.[21-23] From this perspective, $CsPbI_3$ perovskite quantum dots (PQDs) with a few nanometers in size can demonstrate high cubic phase stability and be utilized at RT.[24,25] Adding to strong cubic phase stability, $CsPbI_3$ PQDs have great advantages for solar cell applications. For example, $CsPbI_3$ PQDs have defect tolerance, which enables a high photoluminescence quantum yield up to a near unity without outer shelling and leads to low open-circuit voltage loss in solar cells compared to bulk perovskites.[26-27] Furthermore, $CsPbI_3$ PQDs enable the fabrication of a thick

absorber layer without a thermal annealing process. Therefore, $CsPbI_3$ PQDs are of great interest in photovoltaic absorbers for room-temperature processed next-generation thin film solar cells.

$CsPbI_3$ PQDs are synthesized in colloidal systems with the support of long-chain organic ligands, including oleic acid (OA) and oleylamine (OLA), to control the size, crystallinity, and dispersion properties.[21,28] Although they contribute to the cubic phase stability of $CsPbI_3$ PQDs, the insulating property of long aliphatic chains interferes with charge carrier transfer.[29] By exchanging the insulated long-chain ligands with short acetate ligands through solid-state ligand exchange procedures, in 2016, Luther *et al.* reported $CsPbI_3$ PQD solar cells.[30] Through the advancement of $CsPbI_3$ PQD material and device design strategy, the PCE of $CsPbI_3$ PQD solar cells improved dramatically from 10.77% to 16.2%.[30-35]

Although the device efficiency of $CsPbI_3$ PQD solar cells has improved in the last few years, a central task for their commercialization is to achieve device stability. The factors that affect the stability of $CsPbI_3$ PQD solar cells originate from various issues. The fundamental material factors that cause the instability of $CsPbI_3$ PQD solar cells include the following issues (**Figure 1a**). First, the structural instability of cubic phase $CsPbI_3$ PQDs.[36,37] Despite the high surface-to-volume-ratio and ligand passivation effects, Cs^+ ions constituting $CsPbI_3$-PQDs have fundamentally weak structural stability because the

size of Cs^+ ions is smaller than that of MA^+ and FA^+ ions. Second, $CsPbI_3$ PQDs are highly sensitive to polar solvents because of their inherent ionic nature and dynamic surface.[38,39] When they are exposed to polar media, $CsPbI_3$ PQDs usually lose their optical properties, surface ligands, and even structural integrity.[28,33,34,39,40] Third, due to the low formation energy of $CsPbI_3$ PQDs, they are vulnerable to environmental stress in the conditions with light, oxygen, or heat.[41-43] Thus, environmental stress is considered the most harmful factor affecting the stability of $CsPbI_3$ PQD solar cells. Nevertheless, a lot of studies to overcome the material instability drawbacks of $CsPbI_3$ PQDs, such as surface manipulation and organic-PQD heterostructures, have been actively conducted. Material design strategies to achieve better device stability is illustrated in **Figure 1b** and will be discussed in detail in future sections.

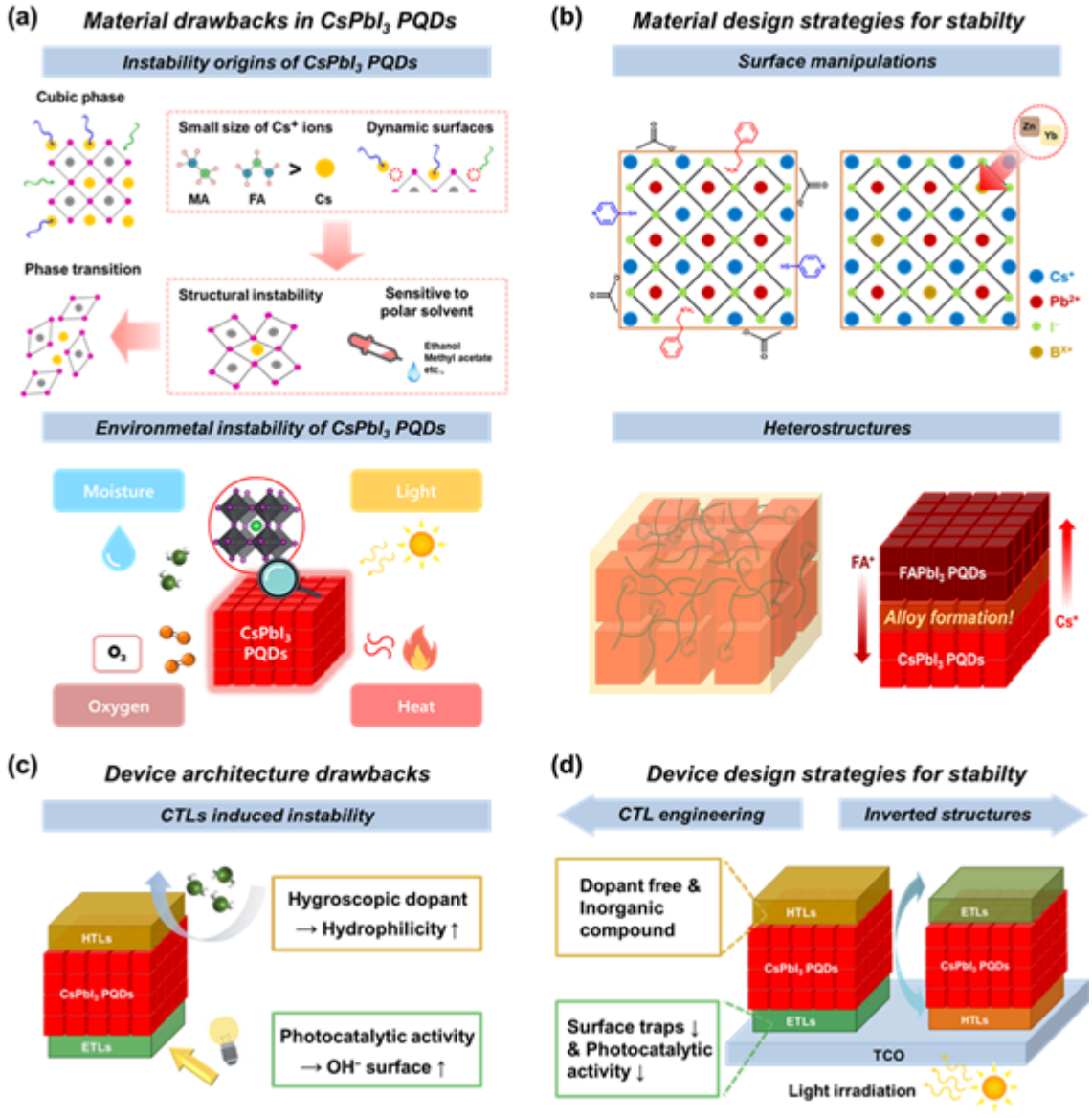

Figure 1. (a) Material factors that impact device stability in $CsPbI_3$ PQDs. (b) Material design strategies for improving device stability. (c) Device architecture drawbacks that induce device instability. (d) Device design strategies for improving device stability.

From the device viewpoint, the device structure of the $CsPbI_3$ PQD solar cells is composed of several functional layers. In general, it is known that each charge transport layer (CTL) plays an important role on the stability of the perovskite solar cells.[44,45] However, existing CTL materials of $CsPbI_3$ PQD solar cells contain hygroscopic species and possess high photocatalytic activity, leading to the formation of numerous defect sites at the interface between the CTLs and $CsPbI_3$ PQD absorbers, causing device instability (**Figure 1c**).[46-48] Device design strategies to overcome device architecture-induced instability is illustrated in **Figure 1d** and will be discussed in detail in future sections.

Improving stability is the main challenge in all PQD-related fields to enhance versatility. Recently, various viewpoints on boost the device efficiency of $CsPbI_3$ PQD solar cells have been reported. However, an in-depth understanding of the degradation of $CsPbI_3$ PQD solar cells induced by the abovementioned issues is required. In this review, we present an overview of the instability origins of $CsPbI_3$ PQD solar cells and recent design strategies for improving solar cell stability from the material and device viewpoints. In addition, several promising solutions, which can further boost the stability of $CsPbI_3$ PQD solar cells, are presented.

2. Material viewpoints on the stability of $CsPbI_3$ PQD solar cells

2.1 Crystallization mechanism of $CsPbI_3$ PQDs

Understanding the formation mechanism of $CsPbI_3$ PQDs is crucial in order to systematically evaluate their stability from a material viewpoint. High-quality and monodispersed $CsPbI_3$ PQDs, which are used as absorber materials in solar cells, are usually pre-crystallized using a hot-injection synthetic method. A brief synthetic pathway of colloidal $CsPbI_3$ PQDs was introduced as follows: (1) Cs-oleate precursors were rapidly injected into a three-necked flask containing PbI_2, octadecene (ODE), and long-chain ligands of OA and OLA at a temperature of about 180℃; (2) After injection, the three-necked flask was quenched to room temperature under ice baths; (3) To remove the excess precursors and precipitate the $CsPbI_3$ PQDs, purification was conducted using mild polar-anti solvents, and finally, the precipitated $CsPbI_3$ PQDs were stored in nonpolar solvents.

During the synthesis and crystallization of $CsPbI_3$ PQDs, nanocrystal nucleation and subsequent growth processes occur. After injection at a high reaction temperature, small nuclei were formed and within a short time, the focusing of size distribution of $CsPbI_3$ PQDs occurs. This crystallization mechanism of $CsPbI_3$ PQDs via colloidal synthetic routes significantly differs from the polycrystalline perovskite films crystallized from the precursor solution through an antisolvent dropping and annealing process on the substrate.[49-51] The classical model of nanocrystal nucleation and growth is the LaMer

mechanism.[52] However, the LaMer mechanism is insufficient to fully explain the nucleation and growth process of $CsPbI_3$ PQDs due to the unique properties of PQDs such as short reaction time scales of PQD formation and complicated components (several precursors and ligands).[53]

Some studies have revealed the detailed formation mechanism of $CsPbI_3$ PQDs. Udayabhaskararao, *et al.* reported the seed-mediated nucleation and growth process of $CsPbI_3$ PQDs as follows:[54] First, PbI_2 dissolved in ODE with OA and OLA ligands forms small spherical seed Pb^0 nanoparticles (NPs). Second, when a Cs-oleate solution was injected into a PbI_2 solution at a high temperature, the spherical NPs grow into $CsPbI_3$:Pb^0 nanocubes (NCs) after 5 s. However, the short-time-scale growth kinetic model of PQDs has not been specifically described.[21] Koolyk, *et al.* suggested the size-focusing and de-focusing kinetics of $CsPbI_3$ PQDs.[55] After Cs-oleate solutions were injected to PbI_2 precursor solutions, $CsPbI_3$ PQDs exhibited the focusing (narrowing) of size distribution in the first 20 s of growth, followed by de-focusing (widening). This is because the diffusion coefficient of iodide is small, so it takes tens of seconds to consume the monomer. Therefore, to obtain high-quality and monodispersed $CsPbI_3$ PQDs for solar cell applications, choosing ab appropriate growth time and monomer concentration is necessary.

Defining the crystallization mechanism of $CsPbI_3$ PQDs can provide insights into

unique properties (including stability) of $CsPbI_3$ PQDs, distinguished from polycrystalline perovskites. However, in-depth studies of this part have not yet been reported, so further studies are needed. In the next section, we discuss the instability origins of $CsPbI_3$ PQDs, crystallized by hot-injection synthesis, from multiple viewpoints.

2.2 Instability origins of $CsPbI_3$ PQDs

2.2.1 Structural instability

The fundamental crystal structure of $CsPbI_3$ PQDs is identical to that of conventional bulk perovskite materials such as methylammonium lead iodide ($MAPbI_3$) with an ABX_3 lattice structure. As shown in **Figure 2a**, the A-site involves an organic or inorganic monovalent cation (Cs^+, MA^+, FA^+, or mixed ions), the B-site involves a metallic divalent cation (Pb^{2+}), and the X site involves a halide anion (Cl^-, Br^-, I^-, or mixed ions).[56] The lattice structure of the cubic $CsPbI_3$ perovskite, which has a photoactive optical bandgap, consists of $[BX_6]^{4-}$ shared octahedral corners and A-site monovalent cations located in large cavities.[57] However, the stability of cubic $CsPbI_3$ is difficult to preserve because of its thermodynamic phase instability that comes from structural limitations.[30,39] To maintain the cubic phase of $CsPbI_3$, the synthesis of PQDs with a nanometer-level crystal size was developed.[21] Due to the high surface tension and size-induced tensile strain of QDs, cubic-phase of $CsPbI_3$ PQDs could be stabilized at RT.[21,22,58] In this section, we evaluate the structural characterization of $CsPbI_3$, its improved cubic phase stability

through a PQD synthesis strategy, and the remaining weaknesses of the PQD structure.

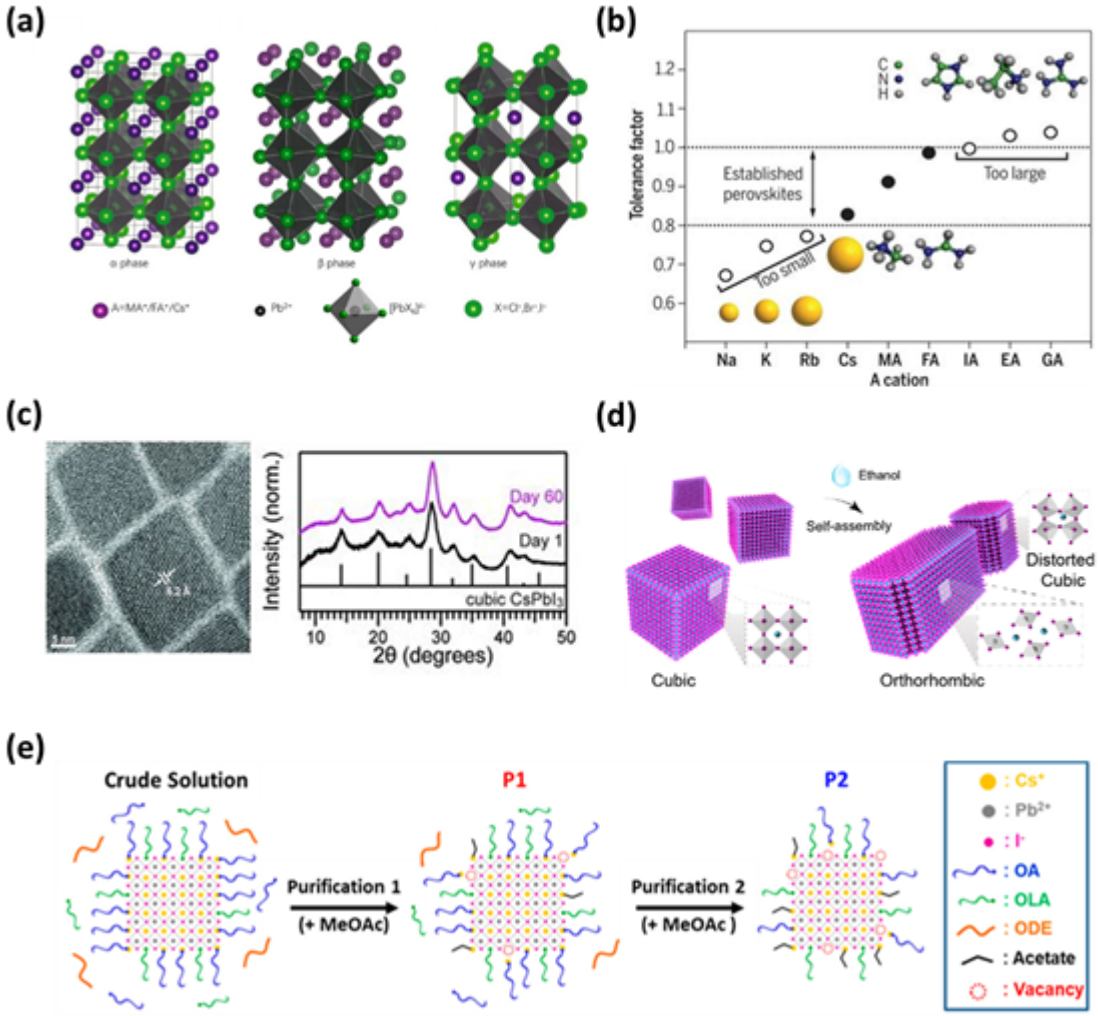

Figure 2. Crystal structure, structural properties, and the dynamic surface of PQDs. a) Typical crystal structures of ABX_3 PQDs. Reproduced with permission.[56] Copyright 2020, Wiley-VCH. (b) Tolerance factor depending on the A-site cation size. Reproduced with permission. [60] Copyright 2017, American Association for the Advancement of Science. (c)

Quantum dot-induced cubic phase stabilization of $CsPbI_3$. Reproduced with permission.[30] Copyright 2016, American Association for the Advancement of Science. (d) Polar solvent-induced lattice distortion of cubic $CsPbI_3$ PQDs. Reproduced with permission.[39] Copyright 2018, American Chemical Society. (e) Purification of an as-synthesized $CsPbI_3$ PQD crude solution using a polar antisolvent, methyl acetate. Reproduced with permission.[34] Copyright 2021, American Chemical Society.

The formation of the perovskite structure depends on temperature, doping, cation/anion size, geometry, and synthesis method.[59] The formed perovskite structure and its stability are dominated by the Goldschmidt tolerance factor (GTF), which can be expressed as GTF = $(R_A + R_X) / \sqrt{2}(R_B + R_X)$, where R_A, R_B, and R_X represents the ionic radius of each site. In general, if the value of GTF lies between 0.9 and 1.0, it is ideal for the cubic perovskite structure with shared octahedral corners, and if the value of GTF lies slightly above 1.0 and below 0.8, hexagonal and orthorhombic phases are common, respectively.[36] Meanwhile, the octahedral factor, μ, is also a considerable criterion for the evaluation of perovskite stability, which is given as $\mu = R_B / R_X$. The value of μ ranging from 0.44 to 0.90 are required for a stable $[PbX_6]^{4-}$ octahedra.[37] Thus, these two factors (GTF and μ) are crucial for the formation of highly stable perovskites and provides valuable insights into developing doping strategies for perovskite materials.

As shown in **Figure 2b**, all-inorganic $CsPbI_3$ perovskites exhibit a GTF (0.81–0.85)

smaller than that of the ideal cubic phase (0.9–1.0), which stems from the smaller ionic radius of Cs^+ compared to those of MA^+ and FA^+ cations.[60] In addition, $CsPbI_3$ has a relatively low octahedral factor (μ = 0.54) resulting from the size of Pb^{2+} and I^-.[61] Therefore, $CsPbI_3$ is difficult to maintain a cubic phase at RT and exists as an orthorhombic phase; thus, it has a wide bandgap of 2.82 eV and cannot acts as a photoactive layer.[17,20] This unfavorable phase can transform into a cubic phase at a high temperature (>320 ℃); however, such a high-temperature condition is undesirable for scalable and flexible device fabrication. To overcome this serious problem, the synthesis of $CsPbI_3$ PQDs is tailored to sustain a cubic phase at RT (**Figure 2c**).[30] The fundamental cause for cubic phase stability of $CsPbI_3$ PQDs remains uncertain, but there are two approaches that attempt to explain this. (1) The OLA ligands contribute to the formation of stable cubic phase of $CsPbI_3$ PQDs as a proton source and to increase the overall GTF.[38,62] (2) The high surface energy and size-induced tensile strain of $CsPbI_3$ PQDs help to maintain their cubic phase at RT.[22,30] However, the weak interaction between the PQD core and the organic ligand may act as an obstacle to maintaining the improved GTF value.[63] Moreover, the high surface-to-volume ratio of PQDs can be compensated by aggregation during purification and film fabrication.[34, 64-66] This can cause distortion in the $CsPbI_3$ PQD lattice and consequently induce a phase transition from the ideal alpha (cubic) to beta or gamma phases and finally to the orthorhombic phase (**Figure 2a**).[56] Therefore, a strategy to maintain a stable surface during purification, ligand exchange,

and film fabrication is essential for the structural stability of $CsPbI_3$ PQDs in device applications.

From a structural viewpoint, the GTF values of $MAPbI_3$ PQDs and $FAPbI_3$ PQDs are 0.91 and 0.99, respectively; thus, their structural stability could exceed that of $CsPbI_3$ PQDs (GTF = 0.81–0.85). However, compared to inorganic Cs-based PQDs, MA and FA-based PQDs exhibit inherent chemical instability. Like bulk perovskite, PQDs with MA or FA in their composition have relatively poor thermal stability due to their organic components.[67] In particular, $MAPbI_3$ PQDs have low formation energy and are readily decomposed even at room temperature, resulting in inevitable conversion to volatile CH_3NH_2, PbI_2, and HI.[68] In addition, MA- and FA-based PQDs are much more susceptible to polar chemicals because the bonding of the monovalent cation (organic molecule) and inorganic cages ($[PbI_6]^{4-}$ octahedra) is relatively weaker than that in inorganic Cs-based PQDs.[69-71] This acts as a fatal drawback for the fabrication process of PQD solar cells (purification and ligand exchange treatment), where using polar chemicals is essential. For these disadvantages, most of the photoactive materials of PQD solar cells reported so far have used Cs-based inorganic PQDs.

2.2.2. Inherent ionic and dynamic nature of $CsPbI_3$ PQDs

$CsPbI_3$ PQDs are not only composed of ionic compounds in their core structure, but their surface interacted with ligands also has ionic characteristics. One of the

important roles of surface ligands is passivation of surface defect sites of PQDs.[72] The functional group head of surface ligands binds to the PQD surface, whereas the long hydrocarbon tail is excluded from the PQDs. However, the surface ligands dynamically bind with the surface of PQDs, representing a weak binding force.[65] Since OA and OLA have relatively weak ionicity due to their long insulating carbon chains, they form weak ionic bonding with the PQD surface and are easily detached by external stimuli.[39,40] This ligand dissociation leads to PQD agglomeration and loss of structural integrity.[28,33,34]

The ionic binding character and the dynamic surface of PQDs lead to their vulnerability to polar solvents (**Figure 2d**). Sun *et al.* observed the phase transition of $CsPbI_3$ PQDs dispersed in high-polarity solvent (ethanol) and stored in ambient conditions.[39] The dark red color of $CsPbI_3$ PQDs gradually turns into yellow, indicating that the cubic phase is transformed into the orthorhombic phase. The atomic-scale structural changes of $CsPbI_3$ PQDs, observed using aberration-corrected scanning transmission electron microscopy (AC-STEM), also demonstrate the phase transition due to polar solvents. This result indicates that polar solvents can induce the lattice distortion of $CsPbI_3$ PQDs, leading to the photoactive cubic phase being transformed into the photoinactive orthorhombic phase, which is undesired for photovoltaics. Moreover, the surface ligands of $CsPbI_3$ PQDs are easily lost during polar antisolvent-based purification.[33,34,40] To produce device-applicable $CsPbI_3$ PQDs, purification steps are necessary to remove excess precursors and ligands. Currently, the most used purification

method involves the precipitation and redissolution method using good solvents for dissolution (i.e., hexane and toluene) and antisolvents for precipitation (i.e., methyl acetate and ethyl acetate). Unfortunately, polar antisolvents induce the removal of capping ligands bounded with the $CsPbI_3$ PQD surface due to the ionic nature of capping ligands. Especially, the soft basic nature of I^- induces weak acid–base interaction with hard acidic OLA ligands, leading to their fast removal during the purification process.[24] As a result of polar antisolvent-based purification, the increase in surface vacant sites and agglomeration of $CsPbI_3$ PQDs are identified (**Figure 2e**).[34] Although $CsPbI_3$ PQDs have a high defect tolerance, increased surface vacant sites cause weak surface states. Therefore, the purification using polar antisolvents chemically weakens the durability of $CsPbI_3$ PQDs for the surrounding environment. In the next section, the influence of the surrounding environment on the stability of the $CsPbI_3$ PQDs is presented.

2.3 Environmental stability

The low stability of perovskite materials under various environmental conditions (oxygen, moisture, heat, light, and so on) is considered a major obstacle to their commercialization.[73] It originates from their volatile organic composition, high defect density, and weak chemical durability.[14,15] In this regard, despite the all-inorganic composition and improved cubic-phase stability, $CsPbI_3$ PQDs still show vulnerability to

the environmental stress. The rapid phase and/or compositional degradation of $CsPbI_3$ PQDs occur when they are exposed to environmental stress through various degradation pathways.[74,75] Therefore, the degradation mechanisms of $CsPbI_3$ PQDs should be analyzed to achieve environmental stability. In this section, we discuss the degradation mechanisms of $CsPbI_3$ PQD solids to develop design strategies for durable $CsPbI_3$ PQD solar cells.

2.3.1 Oxygen- and moisture-induced degradation in $CsPbI_3$ PQDs

In the field of organic–inorganic hybrid perovskites such as $MAPbI_3$, both oxygen- and moisture-derived degradation pathways are well defined. The brief mechanisms of oxygen and water molecules that lead to the degradation of $MAPbI_3$ are proposed respectively as follows. When $MAPbI_3$ thin films are exposed to oxygen under light irradiation, superoxide species are formed because of the photo-induced electron transfer to oxygen molecules which are adsorbed in the iodide vacancies in the $MAPbI_3$ lattice.[76] Reactive superoxide species deprotonate the MA^+ cation; thus, $MAPbI_3$ is decomposed to PbI_2, water, methylamine, and iodine. On the other hand, when $MAPbI_3$ thin films exposed to moisture, the monohydrate $MAPbI_3$ phase is formed.[77] As the hydration accelerates, the dihydrate phase and MAI are formed sequentially. Finally, $MAPbI_3$ is decomposed into MA, HI and PbI_2 irreversibly due to the weak interactions between MA^+ and I^-. As for the all-inorganic $CsPbI_3$ PQDs, the degradation mechanisms

remain controversial. Studies have demonstrated that oxygen-induced degradation is the main pathway for $CsPbI_3$ PQD degradation, while others have suggested that moisture-induced degradation is the main pathway.[74,78]

Moot *et al.* demonstrated detailed mechanisms of how oxygen can participate in the degradation of $CsPbI_3$ PQD films in the presence of water molecules and light irradiation.[78] Iodide-related defects on the $CsPbI_3$ PQD surface can be easily formed after the purification step and the ligand exchange process because of the use of polar antisolvent and imperfect ligand exchange. Then, superoxide species can be generated on the $CsPbI_3$ PQD surface via two routes participated with iodide-related defects (vacancy and interstitial). First, oxygen molecules are adsorbed at the iodide vacancy sites, and photo-induced electron transfer from the $CsPbI_3$ PQDs to adsorbed oxygen molecules leads to the formation of superoxide species on the $CsPbI_3$ PQD surface. Second, iodide interstitials react with oxygen molecules under light irradiation, forming iodide gas molecules and superoxide species (**Figure 3a**). When the superoxide species are generated on the $CsPbI_3$ PQD surface via either route, it reacts with H_2O and forms additional reactive oxygen species (ROS), including perhydroxyl, hydroxide, and hydrogen peroxide. These radical ROS participates in the decomposition of $CsPbI_3$ PQDs to $Pb/CsCO_3$ via various reactions and finally bleaches $CsPbI_3$ PQD films (**Figure 3b**). Although H_2O molecules participate in the formation of destructive species on the $CsPbI_3$ PQD surface, humidity does not further exacerbate the degradation of $CsPbI_3$ PQDs

because the ROS formation reactions require only one H_2O molecule; thus, the presence of a few H_2O molecules is critical, rather than a large amount of H_2O molecules under high humidity.

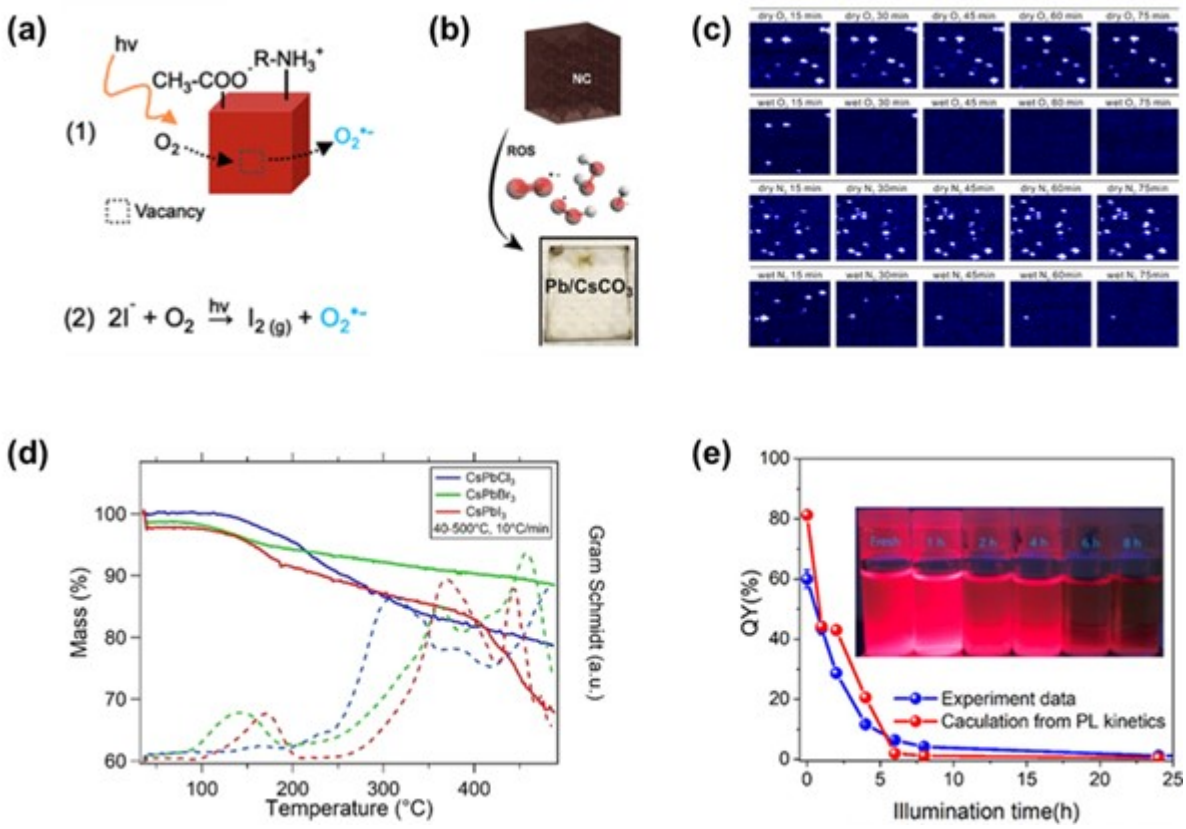

Figure 3. (a) Schematic illustrations of superoxide formation mechanisms in $CsPbI_3$ PQDs. (b) Decomposition of the $CsPbI_3$ PQD film and the photograph of the bleached PQD film. (a,b) Reproduced with permission.[78] Copyright 2020, American

Chemical Society. (c) Continuous confocal scanning PL images of $CsPbI_3$ PQDs in dry and wet conditions. Reproduced with permission.[74] Copyright 2017, American Chemical Society. (d) Mass loss curves for $CsPbX_3$ PQDs from 40 to 500 °C. Reproduced with permission.[79] Copyright 2019, Wiley-VCH. (e) Quantum yield quenching in $CsPbI_3$ PQDs under long-term light illumination. Reproduced with permission.[80] Copyright 2018, American Chemical Society.

In contrast, Yuan, *et al.* asserted that the main pathways for the degradation of $CsPbI_3$ PQDs are induced by moisture and light, rather than oxygen molecules.[74] They measured the PL properties of $CsPbI_3$ PQD films to investigate the degradation mechanism under various environmental conditions. Under the dry nitrogen and oxygen conditions, no change is observed in luminescence intensity, whereas, under the wet nitrogen and oxygen conditions, rapid luminescence degradation occurs in the dark condition (**Figure 3c**), indicating that the moisture, rather than oxygen, induces the degradation of $CsPbI_3$ PQDs. It can be inferred that water molecules easily penetrate the $CsPbI_3$ PQD lattice through surface defects, and damage the structure due to the high polarity of water. Nevertheless, the role of moisture in the degradation of $CsPbI_3$ PQDs still not clearly defined unlike in $MAPbI_3$ perovskites where the hydration reaction accelerates degradation under moisture. Hence, the role of moisture in $CsPbI_3$ PQD degradation should be studied further to clarify the degradation pathway.

2.3.2 Heat-induced degradation in $CsPbI_3$ PQDs

The thermal stability of $CsPbI_3$ PQDs is also an important factor for the stable and long-term operation of solar cells. Boote *et al.* investigated the structural degradation of $CsPbI_3$ PQDs according to elevated temperatures.[79] They found that, among the $CsPbX_3$ PQDs, $CsPbI_3$ PQDs are particularly weak to thermal radiation, whereas the cubic phase degradation of $CsPbBr_3$ and $CsPbCl_3$ PQDs starts at 250 ℃, and $CsPbI_3$ PQDs undergo structural degradation at 50 ℃. The structural degradation of $CsPbX_3$ PQDs at elevated temperatures was investigated by mass loss measurements. $CsPbI_3$ PQDs exhibit rapid mass loss compared to other halide PQDs, resulting from the degradation of surface ligands (**Figure 3d**). It might originate from weak acid–base interactions between I^- and OLA ligands compared to other halide ions.[30] Based on these findings, we speculate that thermal radiation induces surface ligand degradation, leading to instability of $CsPbI_3$ PQDs. Therefore, to enhance the thermal stability of $CsPbI_3$ PQDs, interactions between the $CsPbI_3$ PQD surface and capping ligands can be reinforced.

2.3.3 Light-induced degradation in $CsPbI_3$ PQDs

Solar cells are operated by harvesting incident solar light. Therefore, to achieve the long-term operation stability of $CsPbI_3$ PQD solar cells, the device should have durability under light irradiation. However, the photodegradation of $CsPbI_3$ PQDs under light illumination remains an obstacle to achieving stable $CsPbI_3$ PQD solar cells. An *et al.*

revealed that long-term light illumination causes PL quenching with a serious reduction of PL quantum yield in $CsPbI_3$ PQDs.[80] The detailed photodegradation mechanisms under light illumination are as follows: (1) Light illumination induces detachment of the capping ligands because the photogenerated surface charges can protonate the capping ligands, which then weaken their binding affinity to the surface atoms; (2) Capping ligand detachment leads to surface decomposition, such as the formation of surface dangling bonds; (3) The oxidation state changes from Pb^{2+} to Pb^0 under light illumination, and Pb^0 clusters are formed in $CsPbI_3$ PQDs. Both surface decomposition and Pb^0 clusters act as deep trap states, quenching the PL intensity and quantum yield in $CsPbI_3$ PQDs (**Figure 3e**). Wang *et al.* presented another insight into the photo-induced degradation mechanism in $CsPbI_3$ PQDs.[81] They revealed out that iodine ions migrate out of the $CsPbI_3$ PQD surface under illumination, leading to the formation of iodine vacancies. Moreover, migrated iodine ions can associate with the adjacent Pb^{2+} ions on the $CsPbI_3$ PQD surface, thereby inducing PQD lattice distortion. Owing to iodine vacancies and lattice distortion, the PL intensity of $CsPbI_3$ PQDs significantly decreases under light illumination.

Although more research on the degradation mechanisms of $CsPbI_3$ PQDs is still needed, it is obvious that environmental stresses participate in the degradation pathways of $CsPbI_3$ PQDs, and it becomes more destructive when $CsPbI_3$ PQDs are damaged via various routes (i.e., purification and ligand exchange). Therefore, appropriate material

design strategies are essential to protect the $CsPbI_3$ PQDs from environmental stresses.

2.4 Material design strategies for stable PQD solar cells

2.4.1 Surface manipulation

As mentioned in sections 2.2 and 2.3, the purification and ligand exchange of $CsPbI_3$ PQDs result in severe surface damage. These processes can radically alter surface stoichiometry and eventually damage $[PbI_6]^{4-}$ octahedra, causing numerous surface trap states such as iodide vacancies, and finally deteriorating the stability of $CsPbI_3$ PQD solar cells.[82] Therefore, appropriate surface manipulation strategies such as stable ligand treatments and doping should be introduced during synthesis, purification, and ligand exchange processes to passivate the $CsPbI_3$ PQD surface.

Briefly, introducing short-chain ligands with strong binding energy onto the $CsPbI_3$ PQD surface reinforces interactions between the PQD surface and ligands and increases short-chain ligand coverage on the PQD surface, decreasing surface trap states. In addition, doping $CsPbI_3$ PQDs with anions and/or cations with appropriate ionic radii can not only passivate surface trap states but also improve the GTF and μ value, enhancing the stability of $CsPbI_3$ PQDs as well as corresponding solar cells. From this point of view, we discuss the effects of surface manipulation strategies on the stability of $CsPbI_3$ PQD solar cells in this section.

Undercoordinated Pb^{2+} sites, which are exposed due to the damaged $[PbI_6]^{4-}$ octahedra resulting from ligand desorption, may lead to surface trap states (i.e., iodine vacancies) and structural instability.[82] Doping the B-sites of $CsPbI_3$ PQDs with cations slightly smaller than Pb^{2+} is an effective strategy to enhance the stability of $CsPbI_3$ PQDs by reducing the distortion of $[PbI_6]^{4-}$ octahedra.[83] Thus, a series of studies focused on Zn-doped PQDs by introducing ZnX_2 (X: halide) precursors during the synthesis step of $CsPbI_3$ PQDs. Bi *et al.* used $ZnCl_2$ as a source of Zn^{2+} and Cl^- to enhance the structural stability of $CsPbI_3$ PQDs and passivate the surface iodine vacancies.[84] The incorporation of smaller Zn^{2+} ions into the Pb^{2+} sites causes lattice contraction, which increases the bond strength between Pb and I atoms, reducing the PbI_6 octahedron distortion. Furthermore, the Cl^- ions can passivate the iodide vacancies, reducing nonradiative recombination (**Figure 4a**). As a result, the Zn-doped PQD solar cells retain the PCE over 95% of the initial value after exposure to ambient conditions with 20–30% room humidity (RH) up to 50 h, while the PCE of the non-doped control devices decreases to zero within 25 h. After this work, Zhang *et al.* employed ZnI_2 in the PQD synthesis and developed Zn-doped PQD solar cells.[85] The stability-enhancing effects of Zn doping are similar to those described by Bi *et al*. More importantly, excess I^- ions generated from ZnI_2 reduce iodide vacancies during the PQD synthesis and prevent the formation of new iodide vacancy sites during the fabrication of solar cells. Therefore, ZnI_2-incorporated PQDs exhibit strong cubic phase stability and efficiently reduce charge recombination.

Finally, ZnI_2-incorporated PQD solar cells exhibit a strong device lifetime (10 days) under ambient conditions (RH = 20–30%) (**Figure 4b**). Apart from Zn doping, other doping strategies using Mn or Yb into the B-site of $CsPbI_3$ PQDs have been reported and exhibited similar effects. However, the device performance using Mn- and Yb- doped PQDs did not surpass that of Zn-doped PQD solar cells (**Table 1**). For more stable $CsPbI_3$ PQD solar cells, further studies on doping strategies, such as the introduction of novel metals or mixed halide ions, are required.

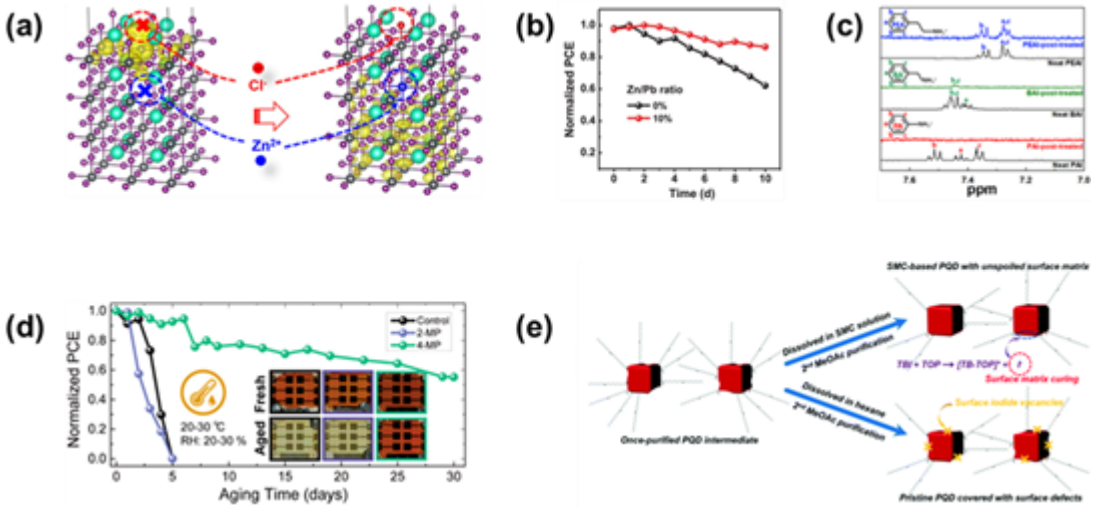

Figure 4. (a) Schematic illustrations of doping into PQDs by introducing $ZnCl_2$. Reproduced with permission.[84] Copyright 2020, American Chemical Society. (b) Long-term stability test of ZnI_2-incorporated PQD solar cells. Reproduced with permission.[85]

Copyright 2020, Wiley-VCH. (c) 1H NMR spectra of PAI, BAI, and PEAI post-treated PQDs. Reproduced with permission.[32] Copyright 2020, Elsevier. (d) Long-term stability test of PQD solar cells based on MeOAc treatment and 2-MP and 4-MP post-treatment. Reproduced with permission.[88] Copyright 2020, American Chemical Society. (e) Schematic illustrations of the surface matrix curing (SMC) treatment of the PQDs based on S_N1 reaction. Reproduced with permission.[35] Copyright 2021, Royal Society of Chemistry.

Table 1. Material design strategies and device stability of $CsPbI_3$ PQD solar cells.

Material design strategy	PCE [%]	Test condition		Retention [%]	Ref. [no.]
		RH [%]	Duration		
Surface manipulation (Yb doping; $YbAc_3$ precursor)	13.12	20-30	150 h	60	83
Surface manipulation	14.8	20-30	50 h	95	84

(Zn doping; $ZnCl_2$ precursor)					
Surface manipulation (Zn doping; ZnI_2 precursor)	16.07	20-30	10 days	85	85
Surface manipulation (Mn doping; precursor)	13.5	Ambient air	7 days	~75	130
Surface manipulation (NaOAc ligand exchange)	12.4	20	20 days	90	131
Surface manipulation (PEAI ligand exchange)	14.1	20-25	15 days	90	32
Surface manipulation (FPEA ligand exchange)	14.65	20-25	15 days	90	87
Surface manipulation (4-MP ligand exchange)	14.25	20-30	30 days	60	88
Surface manipulation	16.21	~10	30 days	83	35

(TOP passivation)					
Heterostructure (Graphene)	11.64	0 (N_2)	720 h	90	66
Heterostructure (PBDB-T)	13.8	20-30	350 h	63	94
Heterostructure ($FAPbI_3$ PQD)	16.07	45-60	1000 h	96	99
Heterostructure (Y6-F)	15.05	20-30	140 h	70	91
Heterostructure (F6TCNNQ)	15.30	20-30	90 h	80	132

We consistently explained that the ligand desorption from the PQD surface is an instability origin of the $CsPbI_3$ PQDs. Thus, direct treatment of short chain ligand with strong binding energy onto PQD surface will be a promising way to enhance the stability of $CsPbI_3$ PQDs. The chemical structure (i.e., substitution position and chain length) of

short chain ligands affect the binding ability onto PQD surface, even if the ligands have same derivative.[86] A series of studies focused on comparing the binding ability of the short chain ligands onto $CsPbI_3$ PQD surface according to their chemical structures to find more strongly binding ligands which can more well passivate the PQD surface, and thereby enhance the stability of $CsPbI_3$ PQD solar cells.

Kim *et al.* introduced a series of phenylalkylammonium cations with different alkyl chain lengths, phenylammonium (PA), benzylammonium (BA), and phenethylammonium (PEA), to replace long-chain OLA ligands.[32] Among them, PA cations that have the shortest alkyl chain cannot substitute OLA ligands. BA and PEA cations can be incorporated into OLA-removed sites; however, the binding ability of BA cations to the $CsPbI_3$ PQD surface is much lower than that of PEA cations, which have longer alkyl chain. As a result, only the PEA cations strongly bind OLA-removed sites and well passivate the $CsPbI_3$ PQD surface (**Figure 4c**). The origin of the relationship between the alkyl chain length of phenylalkylammonium cations and binding ability is not emphasized in this work, but it can be speculated that the short alkyl chain length leads to the steric hindrance of the phenyl group and thus hinders the binding onto the $CsPbI_3$ PQD surface. In addition, PEA cations have a hydrophobic nature; thus, they can protect the $CsPbI_3$ PQD lattice from moisture penetration.[87] Owing to the strong binding of PEA cations onto the $CsPbI_3$ PQD surface and the hydrophobic nature of the phenyl group, the PEA-treated $CsPbI_3$ PQD solar cells show strong stability, retaining over 90% of the initial

performance after 15 days under ambient conditions (RH = 20–25%).

Not only the alkyl chain length but also the substitution position of the functional group in the ligand affects the binding ability of ligands to the $CsPbI_3$ PQD surface. The undercoordinated Pb^{2+} has a soft Lewis acidic nature; thus, it can be passivated using Lewis base ligands. Khan *et al.* reported a PQD surface passivation strategy by employing a series of Lewis bases, o-mercaptopyridine (2-MP) and p-mercaptopyridine (4-MP).[88] Although 2-MP and 4-MP ligands have a Lewis base nature, the binding ability to the $CsPbI_3$ PQD surface is quite different according to the substitution position of the -SH group on the pyridine ring. 2-MP ligands have an ortho-substituting -SH group with the N atom on the pyridine ring; thus, the steric hindrance between the -SH group and the N atom in 2-MP may hinder the binding onto the $CsPbI_3$ PQD surface. On the other hand, a para-substituting -SH group of 4-MP can strengthen the binding ability with Pb^{2+}; therefore, 4-MP can more efficiently passivate the $CsPbI_3$ PQD surface. As a result of the strong binding between 4-MP ligands and the PQD surface, the 4-MP-treated PQD solar cells exhibit decent efficiency after ~30 days under ambient conditions (RH = 20–30%), whereas 2-MP-treated and untreated PQD solar cells lost their photovoltaic performance after 5 days under the same conditions (**Figure 4d**).

So far, we have discussed doping strategies and short-chain ligand treatments that can passivate surface trap states and enhance structural stability during the synthesis

step and the photoactive layer fabrication step (ligand exchange) of $CsPbI_3$ PQDs. However, the $CsPbI_3$ PQD surface can be damaged during the purification step due to the use of polar antisolvents.[33,34,40] Therefore, it is required for effective surface manipulation strategies during the purification step. Jia *et al.* introduced a surface matrix curing (SMC) strategy to recover the surface matrix of PQDs, where iodide vacancies are easily formed during the purification step.[35] To fill in the iodide vacancies of the PQD surface, the unimolecular nucleophilic substitution (S_N1) reaction of tertbutyl iodide (TBI) and the nucleophile triocthylphosphine (TOP) is introduced during the purification step. This S_N1 reaction generates sufficient iodide ions and thus efficiently passivates the iodide vacancies during the second step of purification, restoring the PQD surface matrix (**Figure 4e**). As a result, the TBI·TOP-based PQD solar cells retained 83% of their initial PC E after 30 days (RH = ~10%), whereas the control device retained only 25% of its initial P CE.

2.4.2 Heterostructures

Heterostructures of $CsPbI_3$ PQDs with other components such as organic molecule and PQDs with different composition can be easily obtained due to the facile solution process of PQDs and the film fabrication process based on layer-by-layer deposition. Such heterostructures can be employed in the whole range of PQD solids to passivate the $CsPbI_3$ PQDs or one layer of heterostructures can be inserted in the interface

between $CsPbI_3$ PQDs absorbers and CTLs to improve the interfacial states and device stability. In addition, $FAPbI_3$- and $CsPbI_3$-heterostructured (or bilayerd) PQD solids have recently been employed to enhance the stability of PQD solids. In this section, we discuss the effects of various substances constituting the heterostructured PQDs on device stability and then introduce the stable heterostructured $FAPbI_3/CsPbI_3$ PQD solids that hold great interest in the recent PQD solar cell field.

Wang, *et al.*, introduced micrometer-sized graphene (μGR) sheets to crosslink the PQDs to keep PQDs from agglomeration to achieve long-term stability of PQD solids and corresponding solar cells.[66] Agglomeration of PQDs through recyclable dissolution-recrystallization (purification step) that would turn cubic phase into orthorhombic phase-based film, leading to attenuated stability.[34] Therefore, agglomeration issues of PQDs is not negligible to enhance the device stability. The μGR sheet has functional groups such as hydroxyl, carbonyl, and carboxyl which cause the intermolecular hydrogen bonds between PQDs to μGR, thus it can be possible crosslink μGR and PQDs together. Crosslinking between μGR and PQDs can fix the PQDs in place, thereby preventing the agglomeration of PQDs and phase transition to the orthorhombic phase. Moreover, the hydrophobic nature of μGR prevent efficiently the penetration of moisture to the PQD lattice (**Figure 5a**). Due to the combination of the prevention of PQD agglomeration and hydrophobic nature of μGR, the μGR/PQD solar cells degraded by only 10% of its initial *PCE* under the harsh condition of 60% relative humidity for 5 h. Conjugated organic

molecules have recently been introduced into solar cells to enhance the charge separation ability.[89] In addition, conjugated organic molecules have hydrophobic; thus they can give the moisture resistance property to solar cells.[90] In addition to these properties, in more specific, conjugated organic molecules can passivate the surface trap stats of PQD surface. Yuan, *et al.*, reported PQD/organic molecule hybrid film adopting PQDs and non-fullerene electron acceptor, Y6-F.[91] Y6-F mostly bind with the under-coordinated Pb^{2+} sites which are the surface trap states on PQD surface, thereby it can be possible efficient PQD surface passivation. In more detail, XPS measurement revealed that characteristic peaks of Cs *3d* and Pb *4f* in the Y6-F/PQD hybrid film show a shift to lower binding energies which indicates that the strong interaction between Cs-F and Pb-F, confirming the successful incorporation Y6-F molecules onto the PQD surface (**Figure 5b**). Due to the strong binding between Y6-F and PQDs, the Y6-F/PQD hybrid solar cells exhibited improved device storage stability compared to PQD-only solar cells for 150 h in dry air atmosphere.

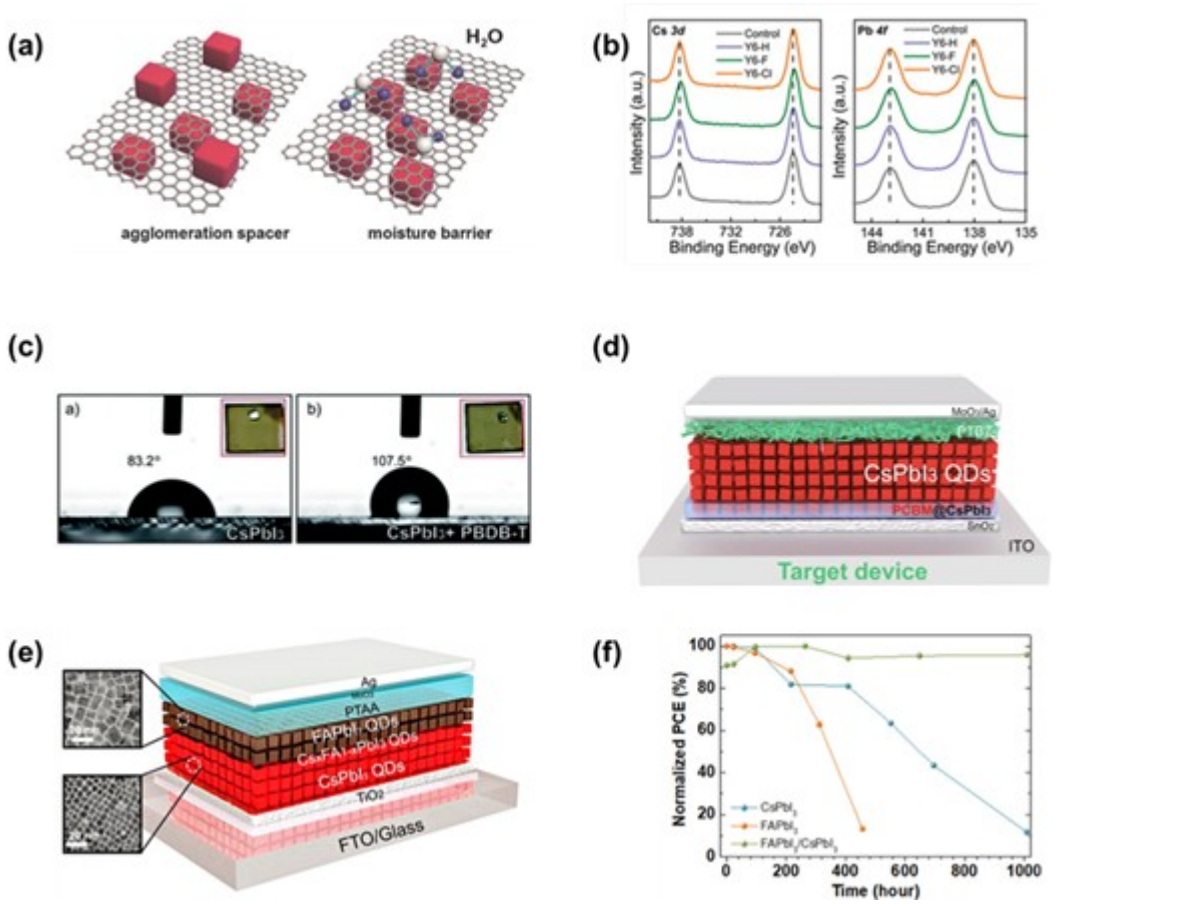

Figure 5. (a) Schematic illustrations of the stabilization mechanism for the μGR/PQDs. Reproduced with permission.[66] Copyright 2018, Wiley-VCH. (b) XPS core-level spectra of PQD films with and without Y6 post-treatment. Reproduced with permission.[91] Copyright 2021, Wiley-VCH. (c) The contact angles between water drops and pristine PQD solids, PBDB-T incorporated PQD solids. Reproduced with permission.[94] Copyright 2020, Royal Society of Chemistry. (d) Schematic diagram of the PQD/PCBM heterostructured solar cells. Reproduced with permission.[95] Copyright 2021. Springer Nature. (e) Schematic

illustration of the bilayer $CsPbI_3$/$FAPbI_3$ PQD solar cell. Reproduced with permission.[98] Copyright 2019, American Chemical Society. (f) Long-term stability test of $CsPbI_3$/$FAPbI_3$ PQD solar cell without encapsulation. Reproduced with permission.[99] Copyright 2020, American Chemical Society.

In addition, the interfaces between photoactive layer and CTLs impact device stability due to the presence of interfacial defects and incompatibility.[92,93] Therefore, to regulate the interfacial properties and improve device stability, one layer of PQDs/polymer heterojuntion has been inserted into the interface between $CsPbI_3$ PQD absorbers and CTLs. Ji *et al* introduced a blended PQDs/PBDB-T heterojunction in the interface between $CsPbI_3$ PQD absorbers and PTAA HTLs.[94] The conjugated polymer PBDB-T was hydrophobic, and therefore stable under ambient conditions. Compared to pristine $CsPbI_3$ PQD solids, the PQDs/PBDB-T heterostructured solids exhibited an increased water-drop contact angle value, indicating that incorporation of PBDB-T into the $CsPbI_3$ PQD solids changes the hydrophilic nature of PQD solids to hydrophobic (**Figure 5c**). Owing to the hydrophobic nature of PBDB-T, the PQDs/PBDB-T heterostructured solar cells exhibited slightly increased device stability under ambient conditions (RH = 20–30%). Similarly, Hu *et al*. introduced one layer of PQDs/PCBM heterostructured solids in the interface between $CsPbI_3$ PQDs and SnO_2 ETLs[95] (**Figure 5d**). PQDs/PCBM heterostructure also exhibited a more hydrophobic nature than the pristine $CsPbI_3$ PQD solids, improving the interfacial contact. Therefore, the PQDs/PCBM-

heterostructured solar cells lost only 30% of their initial PCE value after 14 days under dry air conditions, whereas the control device lost 50% of their initial PCE value.

Recently, organic formamidinium (FA)-incorporated $Cs_{1-x}FA_xPbI_3$ PQDs have attracted great interest as an photoactive layer in the PQD solar cells because FA^+ cation with larger ionic radius than Cs^+ cation can increase tolerance factor of PQDs, improving structural stability.[96,97] The organic-inorganic hybrid $Cs_{1-x}FA_xPbI_3$ PQDs can be easily fabricated by simply combining the $CsPbI_3$ PQD layer and the $FAPbI_3$ PQD layer due to the facile film-state cation exchange between Cs^+ and FA^+ proceeds. Li *et al.* constructed a $CsPbI_3$/$FAPbI_3$ bilayered PQD structure to develop a graded heterojunction.[98] The $FAPbI_3$ PQD layer can protect the $CsPbI_3$ PQD layer because the top $FAPbI_3$ PQDs layer with better structural stability can prevent the moisture penetration into the bottom $CsPbI_3$ PQD layer (**Figure 5e**). Therefore, $CsPbI_3$/$FAPbI_3$ heterojunction PQD solar cells exhibited better device stability compared to homojunction $CsPbI_3$ PQD solar cells under ambient conditions (RH = 20–30%). The role of FA^+ cation on heterostructured PQDs solar cell stability was more clearly defined through sequential research. Park *et al.* demonstrated that in the heterosturctured PQD layer, cation migration between CS^+ and FA^+ occurs, and forming alloyed $Cs_{1-x}FA_xPbI_3$ PQDs.[99] The surface vacancies, which may occurred in the ligand-exchange process, can be passivated thorough this cation migration process. Thus, the trap-assisted recombination is decreased in heterostructured PQD layer compared to mono-compositional PQD layer. This result indicate that during

the cation migration, fast rotated FA^+ can fill in the Cs^+ vacancies which may occur during thin film formation, and finally forming the alloyed $Cs_{1-x}FA_xPbI_3$ PQDs. Through the surface defect passivation via cation migration in heterosturctured PQD layer, the corresponding solar cells retained 96% of their initial *PCE* for over 1000 h under ambient conditions (RH = 45–60%) without encapsulation (**Figure 5f**).

Table 1 summarizes the types of material design strategies, including surface manipulations and heterostructures, as mentioned above, and their effects on the stability of $CsPbI_3$ PQD solar cells. Through these efforts, the device stability of $CsPbI_3$ PQD solar cells have been gradually increased, however, still behind that of bulk perovskite solar cells. To overcome this, new ideas for establishing stable material design strategies are essential. As well as material design, each constituent layer of $CsPbI_3$ PQD solar cells also greatly affects the device stability. In the next section, we discuss the stability of $CsPbI_3$ PQD solar cells from the device viewpoints, such as device architecture and fabrication methods.

3. Device viewpoints on the stability of $CsPbI_3$ PQD solar cells

3.1 Device architecture of the $CsPbI_3$ PQD solar cells

Typical $CsPbI_3$ PQD solar cells consist of five functional parts for efficiently extracting charges generated inside the photoactive layer or at the interface within the device: (1) working electrode, (2) electron transport layer (ETL), (3) photoactive layer, (4)

hole transport layer (HTL) and (5) counter electrode. CTLs located on both sides of the photoactive layer play a role in efficiently extracting photo-generated electrons or holes in the photoactive layer before charge recombination. During device operation, both CTLs affect the stability of $CsPbI_3$ solar cells. Therefore, engineering strategies of each functional parts are important to suppress unexpected carrier recombination and increase the stability of $CsPbI_3$ PQD solar cells. In this section, we discuss the effects of CTLs and device architecture on the stability of $CsPbI_3$ PQD solar cells.

3.1.1 HTL of $CsPbI_3$ PQD solar cells

The HTL material in $CsPbI_3$ PQD solar cells should have an appropriate energy level for PQDs and high hole mobility, which can effectively extract holes and block electrons. Most of the $CsPbI_3$ PQD solar cells reported so far have used 2,2,7,7-tetrakis-(N,N-di-p-methoxyphenylamine)-9,9-bifluorene (Spiro-OMeTAD) or poly(triarylamine) (PTAA) in n-i-p structure. Spiro-OMeTAD is a small organic molecule, an aromatic polyamine compound with a widely distributed electron cloud, which has been widely used in bulk perovskite solar cells.[36, 100-102] Since pure Spiro-OMeTAD has insufficient hole transport ability, it is essential to use dopants such as lithium salt (LiTFSI) and cobalt complex (FK209).[103-105] However, the use of such dopants can accelerate the degradation of perovskite materials under ambient conditions. The degradation mechanism of bulk perovskite by dopants of Spiro-OMeTAD has already been reported in previous

studies.[106-108] Therefore, it is certain that the dopant of spiro-OMeTAD will accelerates the degradation of the photoactive layer even in $CsPbI_3$ PQD solar cells. However, in the $CsPbI_3$ PQD solar cell field, the exact degradation mechanism is not known, so further research is needed. The other HTL generally used in highly efficient $CsPbI_3$ PQD solar cells is PTAA. PTAA interacts more strongly with perovskite at the interface than other hole-conducting polymers, possibly improving hole transfer.[109,110] Ma *et al.* firstly applied PTAA as a HTL material of the $CsPbI_3$ PQD solar cells, and the PTAA-based devices reached an efficiency of 14%, outperforming a range of other semiconducting polymers and spiro-OMeTAD.[111] To date, PTAA has remained a popular choice for the HTL in $CsPbI_3$ PQD solar cells and has been used in many highly efficient devices. However, PTAA is not stable thermally and under moisture due to its inherent organic structure.[112,113] In addition, the use of dopants to achieve high efficiency can also limit the stability of PTAA-based devices. [114,115] To achieve highly stable $CsPbI_3$ PQD solar cells, optimization of HTL is needed. Thus, several approaches have been tried to replace the aforementioned HTLs.

To obtain a highly stable $CsPbI_3$ PQD solar cells, Yuan *et al.* employed organic conjugated polymers, such as PTB7 (**Figure 6a**).[47] Several polymeric hole transport materials (P3HT, PTB7, PTB7-Th) with different energy levels have been tried for efficient electron blocking and hole extraction. When the $CsPbI_3$ PQD film was covered with polymeric hole conductors, the PL strength and lifetime were significantly reduced,

demonstrating that the internal dipole of polymer influence on effective charge extraction and separation. In addition, a better passivation effect was shown in the polymeric hole conductor-covered $CsPbI_3$ PQD film due to the difference in molecular structure and surface morphology. Among several candidates, the $CsPbI_3$ PQD solar cells based on PTB7 as the hole conductor reported a V_{OC} of 1.27V and a high PCE of 12.55%, and the device stability was also greatly improved due to the better passivation and absence of dopants in the HTL. Meanwhile, there has been attempt to improve the stability of $CsPbI_3$ PQD solar cells by using inorganic HTL instead of organic HTL.[48] To address the instability of organic materials induced from inherent chemical structure and hydroscopic additives (Li-TFSI), several inorganic materials (CuI, CuSCN and NiO) have been used in bulk perovskite solar cells.[116] Chen *et al.* employed inorganic $Cu_{12}Sb_4S_{13}$ QDs as a HTL material in $CsPbI_3$ PQD solar cells (**Figure 6b**). They have the advantages of proper valence band energy level, high hole mobility and non-toxicity, as well as being advantageous for hole extraction. As a result, the $Cu_{12}Sb_4S_{13}$ QD-based devices achieved a PCE of 10.02%, and improved long-term stability over the spiro-OMeTAD-based devices. Although the PCE of inorganic HTL-based devices is still low, the excellent long-term stability has shown potential applications in $CsPbI_3$ PQD solar cells.

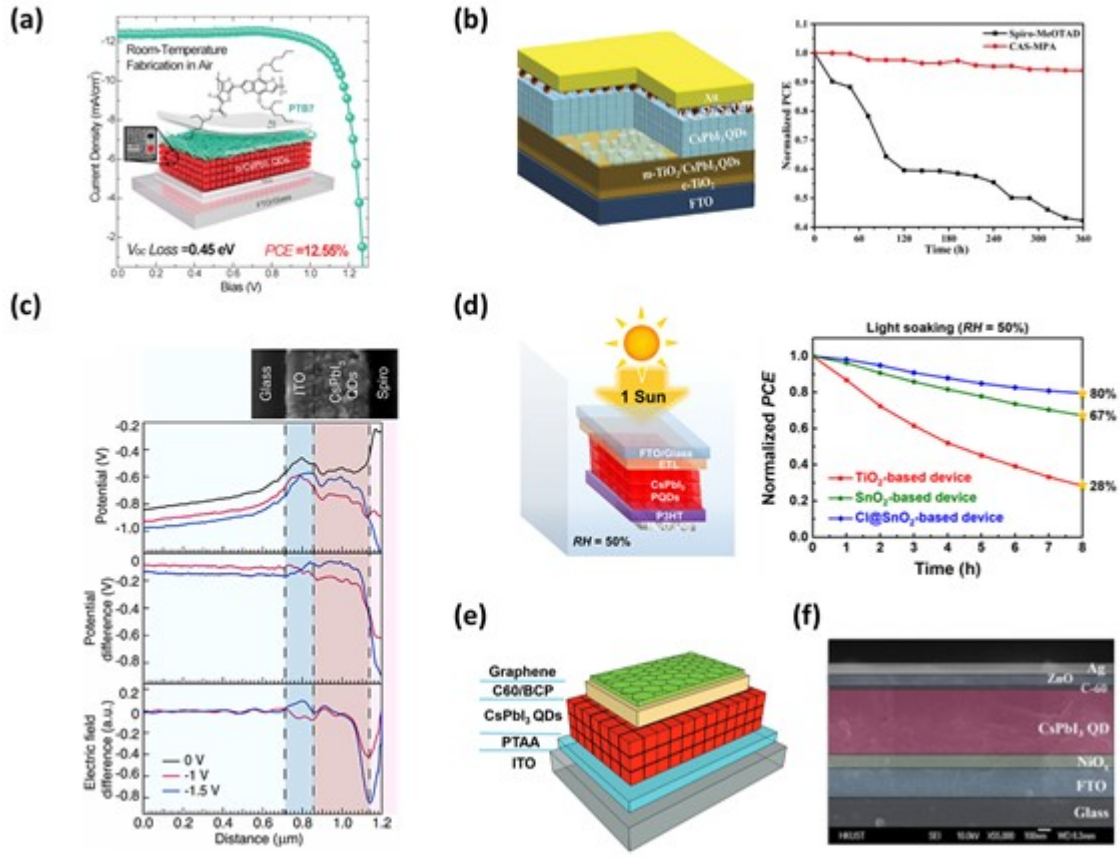

Figure 6. Device design strategies of the $CsPbI_3$ PQD solar cells. (a) $CsPbI_3$ PQD solar cells adopting conjugated polymer hole transport material (PTB7). Reproduced with permission.[47] Copyright 2019, Cell Press. (b) Long-term stability test of $Cu_{12}Sb_4S_{13}$ QD HTL-based $CsPbI_3$ PQD solar cells. Reproduced with permission.[48] Copyright 2020, American Chemical Society. (c) KPFM potential and field profiling results of $CsPbI_3$ PQD solar cells with SnO2 ETL. Copyright 2020, Elsevier. Reproduced with permission.[124] (d) Photostability test of $Cl@SnO_2$ QD ETL-based PQD solar cells. Reproduced with permission.[46] Copyright 2021, American Chemical Society. (e) Schematic illustration of

inverted $CsPbI_3$ PQD solar cells using PTAA and C60/BCP. Reproduced with permission.[119] Copyright 2019, Wiley-VCH. (f) Schematic illustration and SEM images of inverted $CsPbI_3$ PQD solar cells using NiO and C60/ZnO. Reproduced with permission.[129] Copyright 2020, American Chemical Society.

3.1.2 ETL of $CsPbI_3$ PQD solar cells

An ideal ETL material should have good electron mobility and function as a hole-blocking layer to reduce recombination at the ETL/$CsPbI_3$ PQD interface. ETL materials for $CsPbI_3$ PQD solar cells are usually n-type metal oxides (SnO_2, TiO_2, etc.) or small organic molecules (PCBM, C60, etc.) with high electron mobility.[95, 117-119] Among these ETL materials, TiO_2 has an appropriate band structure that matches well with the energy level of $CsPbI_3$ PQDs, making it one of the most widely used ETL materials in $CsPbI_3$ PQD solar cells with an n-i-p structure. However, TiO_2 has low electron mobility and conductivity, and contains oxygen vacancies which induce charge accumulation, recombination, and dissociation. In addition, their high photocatalytic behavior can lowers the stability of the $CsPbI_3$ PQD solar cells during device operation.[46] Therefore, a strategy of using other oxides to overcome the problem of TiO_2 has been presented. SnO_2 is a promising alternative to TiO_2, which has advantages, such as high charge mobility, wide bandgap, and low-temperature processability, and has already been actively used in bulk perovskite solar cells.[120-123] In this point of view, Luther *et al.* introduced a SnO_2 ETL into $CsPbI_3$

PQD solar cells.[124] However, device performance of SnO_2 ETL-based devices was relatively low compared to optimized TiO_2 ETL-based devices. Cross-sectional nanometer-scale Kelvin probe force microscopy (KPFM) analysis revealed that, in this case, the $CsPbI_3$ PQD film failed to effectively form a junction with SnO_2 (**Figure 6c**). This disadvantage could be overcome through improvement of thickness, uniformity, and surface modification in the device process rather than the material limitations of SnO_2. In addition, the effects of ETL on device stability of $CsPbI_3$ PQD solar cells must be deeply analyzed. Choi *et al.* conducted an in-depth study of the effects of TiO_2 and SnO_2 on device stability in $CsPbI_3$ PQD solar cells (**Figure 6d**).[46] They found that TiO_2 ETL can accelerate the cubic-phase degradation of $CsPbI_3$ PQDs under both moisture and light illumination conditions due to its abundant oxygen vacancies and high photocatalytic activity. To address this issue, they developed chloride-passivated SnO_2 nanomaterials, which have few surface traps and low photocatalytic activity, leading suppressed cubic-phase degradation of $CsPbI_3$ PQDs. Moreover, chloride-passivated SnO_2 nanomaterials showed improved electron extraction ability due to the favorable band alignment between the ETL and $CsPbI_3$ PQD absorbers. Owing to these advantages, the $CsPbI_3$ PQD solar cells based on chloride-passivated SnO_2 ETL showed high PCE of 14.5% and significantly improved device operational stability under both ambient and light illumination conditions, compared to those based on TiO_2 ETLs. This result suggests that the stability of $CsPbI_3$ PQD solar cells can be improved through the selection and

modification of ETL materials.

3.1.3 Inverted structure of $CsPbI_3$ PQD solar cells

The device architecture of the $CsPbI_3$ PQD solar cells can be divided into a conventional n-i-p structure and an inverted p-i-n structure according to the positions of the ETL and the HTL. Structural difference of devices can affect the stability of $CsPbI_3$ PQD solar cells. In general, it is known that p-i-n structure perovskite solar cells exhibit less hysteresis and improved device stability.[125] Moreover, p-i-n inverted structures have attractive flexibility, which provides more options for solution-processable inorganic CTLs, resulting in the possibility of obtaining stable $CsPbI_3$ PQD solar cells.[126-128] In 2020, Kong *et al.* reported for the first time a p-i-n inverted $CsPbI_3$ PQD solar cells with a device structure of ITO/PTAA/$CsPbI_3$ PQDs/C60/BCP/Ag (**Figure 6e**).[119] The device efficiency retains 91% of its initial PCE after 14 days under dark (RH = 20%). However, the relatively low device efficiency compared to the n-i-p structure was pointed out as a weakness. The organic HTL can be replaced by NiOx, which can provide better contact between the $CsPbI_3$ PQD absorbers and the HTL.[129] Halpert *et al.* reported $CsPbI_3$ PQD solar cells with a device structure of ITO/NiOx/$CsPbI_3$ PQDs/C60/ZnO/Ag, which showed significantly enhanced PCE of 13.1% (**Figure 6f**). This inverted p-i-n structure $CsPbI_3$ PQD solar cells maintained 80% of the initial PCE after 40 h under the ambient conditions (RH = 30–40%). However, currently achieved stabilities in p-i-n inverted structure $CsPbI_3$ PQD solar

cells remain low compared to the recently reported conventional n-i-p counterparts. Therefore, further studies to develop highly stable p-i-n structured $CsPbI_3$ PQD solar cells are essential, which is expected to play an important role in understanding the mechanisms involved and improving device stability.

Table 2 shows the novel candidates for $CsPbI_3$ PQD solar cell architecture that can replace representative CTLs (TiO_2, spiro-OMeTAD, and PTAA) and conventional structures. These efforts will provide insights into device architectures and CTL material optimization for more stable $CsPbI_3$ PQD solar cells.

Table 2. Device design strategies and the stability of $CsPbI_3$ PQD solar cells.

Device architecture	PCE [%]	Test condition		Retention [%]	Ref. [no.]
		RH [%]	Duration		
FTO/TiO_2/$CsPbI_3$ PQDs/PTB7/Ag	12.55	20–30	35 h	80	47
FTO/c-TiO_2/mTiO_2/ $CsPbI_3$ PQDs/ $Cu_{12}Sb_4S_{13}$ QDs/Au	10.02	Ambient air	360 h	94	48

ITO/SnO_2/$CsPbI_3$ PQDs/ spiro-OMeTAD/Ag	13.66	20	10 days	87	118
FTO/chloride-passivated SnO_2/$CsPbI_3$ PQDs/ spiro-OMeTAD/MoOx/Ag *(Under illumination)	14.5	20–30 (50)	140 h (8 h)	74 (80)	46
ITO/PTAA/$CsPbI_3$ PQDs/C60/BCP/Ag	9.6	20	14 days	91	119
FTO/NiO/$CsPbI_3$ PQDs/ C60/ZnO/Ag	13.10	30–40	40 h	80	129

3.2 Fabrication methods of constituent layers

Like the device architecture, the fabrication method of constituent layers significantly influences solar cell stability. Because the morphology, optical, and electrical properties may vary depending on the manufacture process, even for the same constituent layer. In particular, fabrication methods for realizing more stable CTLs have

been actively reported. Therefore, to enhance the stability of $CsPbI_3$ PQD solar cells, studying the fabrication method of CTLs is essential.

A Solution process is one of the most widely used methods to fabricate CTLs of solar cells, including metal oxides and organic materials.[133-136] It is mainly carried out by applying the manufactured material or inducing a chemical reaction. In general, the CTLs of solar cells are fabricated through the deposition of a precursor solution and thermal annealing. In this process, controlling the annealing temperature or reaction rate of materials can improve the properties of metal oxides such as surface morphology, carrier mobility, and blocking ability.[137-139] J. Ma *et al.* optimized the annealing temperature of a zinc-amine complex solution for fabricating ZnO ETL, improving surface roughness and carrier mobility.[137] The perovskite solar cells fabricated at the optimized annealing temperature (250 °C) maintained 95% of the initial PCE after 288 h in N_2 conditions. E. H. Anaraki *et al.* introduced chemical bath deposition (CBD) of SnO_2 ETL to improve the stability of perovskite solar cells.[138] Through a slow chemical reaction, the CBD process induced the formation of a uniform and pinhole-free SnO_2 layer. This CBD-fabricated SnO_2 ETL improved the surface morphology and blocking ability, resulting in better device stability compared to that of spin-coated SnO_2 ETL. Although the CTLs of $CsPbI_3$ PQD solar cells reported to date are mostly prepared using a solution process, studies on optimizing their manufacturing methods are insufficient. Considering the importance of this on device stability, it seems that related studies are needed in the future.

Chemical vapor deposition (CVD) and atomic layer deposition (ALD) processes are another effective tool to manufacture conformal, uniform, and high-quality CTLs, which have great advantages over the solution process.[140,141] In particular, the ALD process can precisely control monolayer deposition through self-terminating and sequential chemical reactions between more than two components. This self-limiting reaction can achieve uniform and conformal growth of CTLs and buffer layers, which can improve the stability of solar cells. Y. Lee *et al.* introduced a passivated SnO_2 layer on TiO_2 for better surface contact with the perovskite layer.[142] The precisely controlled SnO_2 layer effectively improved the long-term stability of the solar cell, maintaining its initial efficiency over 100 days in ambient conditions without encapsulation. J. Kruszyńska *et al* conducted a study on the characteristics of ETL and device stability by controlling the termination of the AZO layer.[143] Consequently, the perovskite solar cells with a controlled ALD–AZO layer showed better moisture stability than ZnO-based perovskite solar cells, which maintained more than 80% of initial efficiency after 100 h under 40% relative humidity without encapsulation. Although the ALD technique has not yet been applied in the PQD solar cell field, it has been used in other optoelectronic devices, such as LEDs. Yun *et al.* reported $CsPbBr_3$ PQD LEDs fabricated by deposition of Al_2O_3 and ZnO via ALD to prevent polar solvent-induced damage during the spin coating of ETL.[144] Similar to its passivation of the PQD surface, Al_2O_3 layer prevented PL quenching because it was deposited at low temperatures. Considering these results, since $CsPbI_3$ PQD solar cells

use a similar CTL of bulk perovskite solar cells and PQD LEDs, the ALD technique seems to be sufficiently applicable to $CsPbI_3$ PQD solar cells. In particular, the advantages of ALD's sophisticated thickness control and prevention of damage to the lower layer in the deposition process are thought to induce improved device stability and process advantages when applied to $CsPbI_3$ PQD solar cells.

4. Conclusions and perspectives

$CsPbI_3$ PQDs have shown great potential as absorbers in solution processed next-generation solar cells due to their outstanding photovoltaic properties. Through novel and tremendous efforts, the photovoltaic performance of $CsPbI_3$ PQD solar cells has been achieved up to a PCE of 16.2%, which makes them competitive for rapid commercialization; however, their poor material and device stability remains a major obstacle to their versatility. Therefore, analyzing and understanding the degradation mechanisms of $CsPbI_3$ PQDs and corresponding solar cells give insights into the design strategies to enhance device stability.

In this review, we summarized the key factors which cause the instability of $CsPbI_3$ PQD solar cells and strategies for enhancing the stability by dividing the categories into the materials and devices. In terms of materials instability, the relatively small GTF and μ value, ionic nature, and dynamic surface of $CsPbI_3$ PQDs can cause structural and surface damage. The destructive species such as oxygen and water molecules can easily

penetrate the damaged $CsPbI_3$ PQD lattice and cause phase and/or compositional degradation under ambient conditions through various degradation pathways. Therefore, appropriate material design strategies are necessary to recover the damaged $CsPbI_3$ PQDs. For example, surface manipulation strategies, such as doping metal and using short-chain ligands, were introduced to reinforce the structural stability and surface passivation. Moreover, organic-PQD heterostructure was also contribute to enhance the device stability of $CsPbI_3$ PQD solar cells.

Not only the inherent properties of $CsPbI_3$ PQDs, but also device architecture affects the instability of $CsPbI_3$ PQD solar cells. $CsPbI_3$ PQD solar cells are constituted of various functional layers such as HTL and ETL. These layers are essential for the efficient charge transport; however, vulnerable organic material-based HTLs and metal oxide-based ETLs with numerous oxygen vacancies are pointed out as factors inducing the device instability. To solve the functional layer-based device instability problems, alternative CTLs, such as SnO_2 and PTB7, introduced to $CsPbI_3$ PQD solar cells. In addition, inverted p-i-n structure PQD solar cells can give the chance to enhance the device stability. Meanwhile, the methods for fabricating constituent layers of solar cells have been discussed. The novel deposition technique, such as ALD, was mentioned as a potential candidate for improving device stability.

Through these efforts to investigate the origin of instability and enhance the

stability of $CsPbI_3$ PQDs and corresponding solar cells, the device stability of PQD solar cells under ambient conditions dramatically increased. However, the device stability of $CsPbI_3$ PQD solar cells is relatively poor compared to that of bulk perovskite solar cells. In particular, compared to bulk perovskite solar cells with operational long-term stability over 1000 h under real operating condition, the continuous operational stability of $CsPbI_3$ PQD solar cells is still too low (few minute scale). Moreover, environmental controls such as low humidity is still required to measure the photovoltaic performance of $CsPbI_3$ PQD solar cells. Therefore, it is essential to develop effective strategies for more durable $CsPbI_3$ PQD solar cells with operational long-term stability to endure in real operating condition, such as ambient conditions with continuous light illumination. For more durable operation of $CsPbI_3$ PQD solar cells, the following strategies should be developed:

(1) Finding the most suitable composition for stable $CsPbI_3$ PQD solar cells: Although $CsPbI_3$ PQDs demonstrate a suitable bandgap for solar cell applications, instability is caused by inadequate GTF value. Br alloy can alleviate the problem, but it can increase the bandgap and affect the electronic structure, resulting in efficiency drop. Mixing Cs and FA not only improves the cubic-phase stability but also optimizes their optoelectronic properties. However, using organic molecules has a disadvantage in that the thermal stability of PQDs may be reduced. Thus, instead of organic molecules, it is necessary to find an A-site alloy metal that can overcome the low tolerance factor due to the small size of Cs. B-site doping can simultaneously improve efficiency and stability

while maintaining the inorganic composition of PQDs. So far, Zn has been considered as the most promising candidate, but it needs to be further improved through the application of other metals in the future.

(2) Development of the best ligand for stable $CsPbI_3$ PQD solar cells: Ligands play a key role in the stability of the $CsPbI_3$ PQDs and final device performance. The existing ligand pairs (OA and OLA) used for PQD synthesis have highly dynamic surface, leading to the degradation of $CsPbI_3$ PQDs by water and oxygen molecules. Various ligands have been applied to overcome this, but the development of the ligands that improve both stability and efficiency simultaneously is yet to be seen. Therefore, it is necessary to search for ligands that are shorter in length, have stronger interactions with PQDs, and have environmental stability. This will become possible either through direct synthesis using new types of ligands or through liquid- and solid-state ligand exchange treatments.

(3) Development of the polar solvent-free solar cell fabrication process: To fabricate high-efficiency $CsPbI_3$ PQD solar cells, polar antisolvent-based processes, including purification and ligand exchange, are essential so far. However, as we have consistently noted, polar antisolvents, such as methyl acetate and ethyl acetate, cause surface vacant sites and agglomeration of $CsPbI_3$ PQDs with a highly ionic and dynamic surface nature, leading to stability deterioration in $CsPbI_3$ PQD solar cells. Therefore, a polar solvent-free process should be developed to enhance the stability of materials and

solar cells. To achieve a polar solvent-free process, the currently used precipitation–redissolution purification method and solid-state ligand exchange process should be replaced. It is very challenging; thus, novel ideas are needed to develop a polar solvent-free solar cell fabrication process

(4) Enhancing the robustness of $CsPbI_3$ PQDs structure: Growing epitaxial shells over the core of QDs can efficiently passivate the surface defects and enhance structural robustness of QDs. In the field of chalcogenide QDs, core/shell structures have been widely adopted to improve the stability of QDs. From this point of view, some groups have tried to implement the core/shell structure in $CsPbI_3$ PQDs to improve the material stability.[145,146] However, the development of core/shell structured $CsPbI_3$ PQDs is still limited due to the highly dynamic surface and ionic nature of PQDs.[147] In addition, the shell of $CsPbI_3$ PQDs must be thin enough for smooth carrier transport. Therefore, the development of novel synthetic strategies that can overcome these limitations is required.

(5) Development of active layer deposition techniques: Currently, solid-state ligand exchange based on layer-by-layer deposition via spin-coating is almost the only method to fabricate thick and conductive $CsPbI_3$ PQD absorbers for high-efficiency solar cells. During the layer-by-layer deposition, the long-chain capping ligands are repeatedly exchanged with short-chain ligands, causing volumetric shrinkage and cracking of the $CsPbI_3$ PQD absorber film.[148] Moreover, numerous surface trap states are formed due to

imperfect passivation during the layer-by-layer deposition.[149] Consequently, the layer-by-layer deposition method can damage the absorber film and cause the degradation of $CsPbI_3$ PQDs. Despite these shortcomings, studies on deposition techniques that can replace currently used layer-by-layer method are still lacking. Therefore, the development of advanced deposition techniques, such as one-step deposition method based on solution-phase ligand exchange, should be actively conducted.

(6) Encapsulation strategies using other materials: The heterostructure of $CsPbI_3$ PQDs and organic materials has been widely used to improve device stability. A protective layer covering $CsPbI_3$ PQDs can prevent direct contact with moisture and oxygen, giving excellent stability. In addition, organic materials with functional groups capable of interacting with the $CsPbI_3$ PQD surface can be hybridized with $CsPbI_3$ PQDs to passivate the surface to improve surface stability. However, the thermal stability of heterostructure strategies using organic materials is still limited. The encapsulation strategies using inorganic materials, such as nanocomposite integrated structure and embedding structure in perovskite matrix, can be a promising alternative. Since inorganic materials are compact and thermally stable, they have a potential to effectively encapsulate $CsPbI_3$ PQDs, and more studies are required in this direction.

(7) Optimization of ETL and HTL (materials and fabrication methods) for stable $CsPbI_3$ PQD solar cells: Carrier recombination at the interface between the photoactive

layer and the CTLs can lead to a decrease in device stability as well as efficiency, which should be suppressed through effective CTL development. In addition, as the most widely used CTL material, the photocatalytic activity of TiO_2 (ETL) and dopant use of spiro-OMeTAD and PTAA (HTL) are directly responsible for the instability of PQD solar cells. Optimizing the fabrication methods of CTLs, especially deposition technique, are also needed to improve device stability. Therefore, the development of stable CTL is required, such as low-temperature-processed metal oxide ETLs, dopant-free HTL materials, and using ALD technique.

These promising strategies have the potential to improve the device stability of $CsPbI_3$ PQD solar cells, leading to durable $CsPbI_3$ PQD solar cells with operational long-term stability. With the operational long-term stability goal achieved, we believe that $CsPbI_3$ PQDs will be successfully commercialized in the near future.

Acknowledgements

S. Lim and S. Han contributed equally to this work. This work was supported by the National Research Foundation of Korea (NRF) grant funded by the Ministry of Science and ICT (MSIT) (No. 2021R1A5A1084921, No. 2021R1A2C3004420, No. 2020R1C1C1012256).

WILEY-VCH

Received: ((will be filled in by the editorial staff))

Revised: ((will be filled in by the editorial staff))

Published online: ((will be filled in by the editorial staff))

References

[1] H. Min, D. Y. Lee, J. Kim, G. Kim, K. S. Lee, J. Kim, M. J. Paik, Y. K. Kim, K. S. Kim, M. G. Kim, T. J. Shin, S. I. Seok, *Nature* **2021**, *598*, 444.

[2] H. Kim, L. Zhao, J. S. Price, A. J. Grede, K. Roh, A. N. Brigeman, M. Lopez, B. P. Rand, N. C. Giebink, *Nat. Commun.* **2018**, *9*, 4893.

[3] H. Jing, R. Peng, R.-M. Ma, J. He, Y. Zhou, Z. Yang, C.-Y. Li, Y. Liu, X. Guo, Y. Zhu, D. Wang, J. Su, C. Sun, W. Bao, M. Wang, *Nano Lett.* **2020**, *20*, 7144.

[4] N. G. Park, *Materials today* **2015**, *18*, 65.

[5] S. D. Stranks, G. E. Eperon, G, Grancini, C. Menelaou, M. J. P. Alcocer, T. Leijtens, L. M. Herz1, A. Petrozza, H. J. Snaith, *Science* **2013**, *342*, 341.

[6] S.-H. Turren-Cruz, M. Saliba, M. T. Mayer, H. Jua´rez-Santiesteban, X. Mathew, L. Nienhaus, W. Tress, M. P. Erodici, M. J. Sher, M. G. Bawendi, M. Grätzel, A. Abate, A. Hagfeldt, J.-P. Correa-Baena, *Energy Environ. Sci.* **2018**, *11*, 78.

[7] K. X. Steirer, P. Schulz, G. Teeter, V. Stevanovic, M. Yang, K. Zhu, J. J. Berry, *ACS Energy Lett.* **2016**, *1*, 360.

[8] J. Burschka, N. Pellet, S.-J. Moon, R. Humphry-Baker, P. Gao, M. K. Nazeeruddin, M. Grätzel, *Nature* **2013**, *499*, 316.

[9] M. Liu, M. B. Johnston, H. J. Snaith, *Nature* **2013**, *501*, 395.

[10] N. J. Jeon, J. H. Noh, W. S. Yang, Y. C. Kim, S. Ryu, J. Seo, S. I. Seok, *Nature* **2015**, *517*, 476.

[11] W. S. Yang, B.-W. Park, E. H. Jung, N. J. Jeon, Y. C. Kim, D. U. Lee, S. S. Shin, J. Seo, E. K. Kim, J. H. Noh, S. I. Seok, *Science* **2017**, *356*, 1376.

[12] NREL efficiency chart

[13] B.-W. Park, S. I. Seok, *Adv. Mater.* **2019**, *31*, 1805337.

[14] J. A. Christians, P. A. Miranda Herrera, P. V. Kamat, *J. Am. Chem. Soc.* **2015**, *137*, 1530.

[15] E. J. Juarez-Perez, Z. Hawash, S. R. Raga, L. K. Ono, Y. Qi, *Enegy Envirn. Sci.* **2016**, *9*, 3406.

[16] S. I. Rahman, B. S. Lamsal, A. Gurung, A. H. Chowdhury, K. M. Reza, N. Ghimire, B. Bahrami, W. Luo, R. S. Bobba, J. Pokharel, A. Baniya, A. R. Laskar, K. Emshadi, M. T. Rahman, Q. Qiao, *ACS Appl. Mater. Interfaces* **2020**, *12*, 41312.

[17] G. E. Eperon, G. M. Paternò, R. J. Sutton, A. Zampetti, A. A. Haghighirad, F. Cacialli, H. J. Snaith, *J. Mater. Chem. A* **2015**, *3*, 16988.

[18] J. Liang, C. Wang, Y. Wang, Z. Xu, Z. Lu, Y. Ma, H. Zhu, Y. Hu, C. Xiao, X. Yi, G. Zhu, H. Lv, L. Ma, T. Chen, Z. Tie, Z. Jin, J. Liu, *J. Am. Chem. Soc.* **2016**, *138*, 15829.

[19] S. M. Yoon, H. Min, J. B. Kim G. Kim, K. S. Lee, S. I. Seok, *Joule* **2021**, *5*, 183.

[20] C. C. Stoumpos, M. G. Kanatzidis*, Acc. Chem. Res.* **2015**, *48*, 2791.

[21] L. Protesescu, S. Yakunin, M. I. Bodnarchuk, F. Krieg, R. Caputo, C. H. Hendon, R. X. Yang, A. Walsh, M. V. Kovalenko, *Nano Lett.* **2015**, *15*, 3692.

[22] Q. Zhao, A. Hazarika, L. T. Schelhas, J. Liu, E. A. Gaulding, G. Li, M. Zhang, M. F. Toney, P. C. Sercel, J. M. Luther, *ACS Energy Lett.* **2019**, *5*, 238.

[23] R. X. Yang, L. Z. Tan, *J. Chem. Phys.* **2020**, *152*, 034702.

[24] F. Liu, Y. Zhang, C. Ding, S. Kobayashi, T. Izuishi, N. Nakazawa, T. Toyoda, T. Ohta, S. Hayase, T. Minemoto, K. Yoshino, S. Dai, Q. Shen, *ACS Nano* **2017**, *11*, 10373.

[25] A. Dutta, S. K. Dutta, S. D. Adhikari, N. Pradhan, *Angew. Chem. Int. Ed.* **2018**, *57*, 9083.

[26] M. V. Kovalenko, L. Protesescu, M. I. Bodnarchuk, *Science* 2017, 358, 745.

[27] B. M. Wieliczka, J. A. Márquez, A. M. Bothwell, Q. Zhao, T. Moot, K. T. VanSant, A. J. Ferguson, T. Unold, D. Kuciauskas, J. M. Luther, *ACS Nano* 2021, 15, 19334.

[28] Y. Zhang, T. D. Siegler, C. J. Thomas, M. K. Abney, T. Shah, A. D. Gorostiza, R. M. Greene, B. A. Korgel, *Chem. Mater.* **2020**, *32*, 5410.

[29] X. Ling, J. Yuan, X. Zhang, Y. Qian, S. M. Zakeeruddin, B. W. Larson, Q. Zhao, J. Shi, J. Yang, K. Ji, Y. Zhang, Y. Wang, C. Zhang, S. Duhm, J. M. Luther, M. Grätzel, W. Ma, *Adv. Mater.* **2020**, *32*, 2001906.

[30] A. Swarnkar, A. R. Marshall, E. M. Sanehira, B. D. Chernomordik, D. T. Moore, J. A. Christians, T. Chakrabarti, J. M. Luther, *Science* **2016**, *354*, 92.

[31] E. M. Sanehira, A. R. Marshall, J. A. Christians, S. P. Harvey, P. N. Ciesielski, L. M. Wheeler, P. Schulz, L. Y. Lin, M. C. Beard, J. M. Luther, *Sci. Adv.* **2017**, *3*, eaao4204.

[32] J. Kim, S. Cho, F. Dinic, J. Choi, C. Choi, S. M. Jeong, J.-S. Lee, O. Voznyy, M. J. Ko, Y. Kim, *Nano Energy* **2020**, *75*, 104985.

[33] Y. Wang, J. Yuan, X. Zhang, X. Ling, B. W. Larson, Q. Zhao, Y. Yang, Y. Shi, J. M. Luther, W. Ma, *Adv. Mater.* **2020**, *32*, 2000449.

[34] S. Lim, G. Lee, S. Han, J. Kim, S. Yun, J. Lim, Y.-J. Pu, M. J. Ko, T. Park, J. Choi, Y. Kim, *ACS Energy Lett.* **2021**, 6, 2229.

[35] D. Jia, J. Chen, X. Mei, W. Fan, S. Luo, M. Yu, J. Liu, X. Zhang, *Energy Environ. Sci.* **2021**, *14*, 4599.

[36] M. Saliba, T. Matsui, K. Domanski, J.-Y. Seo, A. Ummadisingu, S. M. Zakeeruddin, J.-P. Correa-Baena, W. R. Tress, A. Abate, A. Hagfeldt and M. Grätzel, *Science* **2016**, *354*, 206.

[37] M. A. Green, A. Ho-Baillie, H. J. Snaith, *Nat. Photonics* **2014**, *8*, 506.

[38] L. M. Wheeler, E. M. Sanehira, A. R. Marshall, P. Schulz, M. Suri, N. C. Anderson, J. A. Christians, D. Nordlund, D. Sokaras, T. Kroll, S. P. Harvey, J. J. Berry, L. Y. Lin, J. M. Luther, *J. Am. Chem. Soc.* **2018**, *140*, 10504.

[39] J.-K. Sun, S. Huang, X.-Z. Liu, Q. Xu, Q.-H. Zhang, W.-J. Jiang, D.-J. Xue, J.-C. Xu, J.-Y. Ma, J. Ding, *J. Am. Chem. Soc.* **2018**, *140*, 11705.

[40] Y. Kim, E. Yassitepe, O. Voznyy, R. Comin, G. Walters, X. Gong, P. Kanjanaboos, A. F. Nogueira, E. H. Sargent, *ACS Appl. Mater. Interfaces* **2015**, *7*, 25007.

[41] M. Lorenzon, L. Sortino, Q. Akkerman, S. Accornero, J. Pedrini, M. Prato, V. Pinchetti, F. Meinardi, L. Manna, S. Brovelli, *Nano Lett.* **2017**, *17*, 3844.

[42] N. D. Cottam, C. Zhang, J. L. Wildman, A. Patanè, L. Turyanska, O. Makarovsky, *Adv. Optical Mater.* **2021**, *9*, 2100104.

[43] M. Liu, Q. Wan, H. Wang, F. Carulli, X. Sun, W. Zheng, L. Kong, Q. Zhang, C. Zhang, Q. Zhang, S. Brovelli, L. Li, *Nat. Photonics* **2021**, *15*, 379.

[44] M. Spalla, L. Perrin, E. Planes, M. Matheron, S. Berson, L. Flandin, *ACS Appl. Energy Mater.* **2020**, *3*, 3282.

[45] J. A. Christians, P. Schulz, J. S. Tinkham, T. H. Schloemer, S. P. Harvey, B. J. Tremolet de Villers, A. Sellinger, J. J. Berry, J. M. Luther, *Nat. Energy* **2018** *3*, 68.

[46] S. Lim, J. Kim, J. Y. Park, J. Min, S. Yun, T. Park, Y. Kim, J. Choi, *ACS Appl. Mater. Interfaces* **2021**, *13*, 6119.

[47] J. Yuan, X. Ling, D. Yang, F. Li, S. Zhou, J. Shi, Y. Qian, J. Hu, Y. Sun, Y. Yang, X. Gao, S. Duhm, Q. Zhang, W. Ma, *Joule* **2018**, *2*, 2450.

[48] Y. Liu, X. Zhao, Z. Yang, Q. Li, W. Wei, B. Hu, W. Chen, *ACS Appl. Energy Mater.* **2020**, *3*, 3521.

[49] Z. Xing, S. Lin, X. Meng, T. Hu, D. Li, B. Fan, Y. Cui, F. Li, X. Hu, Y. Chen, *Adv. Funct. Mater.* **2021**, *31*, 2107726.

[50] Z. Xing, X. Meng, D. Li, T. Hu, X. Hu, Y. Chen, *Sci. Bull.* **2022**, *67*, 561.

[51] M. Jung, S.-G. Ji , G. Kim, S. I. Seok, *Chem. Soc. Rev.* **2019**, *48*, 2011.

[52] N. T. K. Thanh, N. Maclean, S. Mahiddine. *Chem. Rev.* **2014**, *114*, 7610.

[53] J. C. Sadighian, C. Y. Wong, *J. Phys. Chem. C* **2021**, *125*, 20772.

[54] T. Udayabhaskararao, M. Kazes, L. Houben, H. Lin, D. Oron, *Chem. Mater.* **2017**, *29*, 1302.

[55] M. Koolyk, D. Amgar, S. Aharona, L. Etgar, *Nanoscale* **2016**, *8*, 6403.

[56] Y. Zhao, J. Li, Y. Dong, J. Song, *Isr. J. Chem.* **2019**, *59*, 649.

[57] C. K. Møller, *Nature* **1958**, *182*, 1436.

[58] R. X. Yang, L. Z. Tana, *J. Chem. Phys.* **2020**, *152*, 034702.

[59] X. Xu, X. Wang, *Small Struct.* **2020**, *1*, 2000009.

[60] J.-P. Correa-Baena, M. Saliba, T. Buonassisi, M. Grätzel, A. Abate, W. Tress, A. Hagfeldt, *Science* **2017**, *358*, 739.

[61] C. Li, X. Lu, W. Ding, L. Feng, Y. Gao, Z. Guo, *Acta Crystallogr., Sect. B: Struct. Sci.* **2008**, *64*, 702.

[62] S. ten Brinck, I. Infante, *ACS Energy Lett.* **2016**, *1*, 1266.

[63] Z. Liu, Y. Bekenstein, X. Ye, S. C. Nguyen, J. Swabeck, D. Zhang, S. T. Lee, P. Yang, W. Ma, A. P. Alivisatos, *J. Am. Chem. Soc.* **2017**, *139*, 5309.

[64] W. Gao, C. Ran, J. Xi, B. Jiao, W. Zhang, M. Wu, X. Hou , Z. Wu, ChemPhysChem, **2018**, *19*, 1696.

[65] J. De Roo, M. Ibáñez, P. Geiregat, G. Nedelcu, W. Walravens, J. Maes, J. C. Martins, I. Van Driessche, M. V. Kovalenko, Z. Hens, *ACS Nano* **2016**, 10, 2071.

[66] Q. Wang, Z. Jin, D. Chen, D. Bai, H. Bian, J. Sun, G. Zhu, G. Wang, S. F. Liu, *Adv. Energy Mater.* **2018**, *8*, 1800007.

[67] Q. A. Akkerman, G. Rainò, M. V. Kovalenko, L. Manna, *Nat. Mater.* **2018**, *17*, 394.

[68] L. Protesescu, S. Yakunin, S. Kumar, J. Bär, F. Bertolott, N. Masciocchi, A. Guagliardi, M. Grotevent, I. Shorubalko, M. I. Bodnarchuk, C.-J. Shih, M. V. Kovalenko, *ACS Nano* **2017**, *11*, 3119.

[69] J.-W. Lee, D.-H. Kim, H.-S. Kim, S.-W. Seo, S. M. Cho, N.-G. Park, *Adv. Energy Mater.* **2015**, *5*, 1501310.

[70] H. Zhu, K. Miyata, Y. Fu, J. Wang, P. P. Joshi, D. Niesner, K. W. Williams, S. Jin, X.-Y. Zhu, *Science* **2016**, *353*, 1409.

[71] M. Kulbak, S. Gupta, N. Kedem, I. Levine, T. Bendikov, G. Hodes, D. Cahen, *J. Phys. Chem. Lett*. **2016**, *7*, 167.

[72] V. K. Ravi, P. K. Santra, N. Joshi, J. Chugh, S. K. Singh, H. Rensmo, P. Ghosh, A. Nag, *J. Phys. Chem. Lett.* **2017**, 8, 4988.

[73] L. Qiu, L. K.Ono, Y. Qi, *Mater. Today Energy* **2018**, *7*, 169.

[74] G. Yuan, C. Ritchie, M. Ritter, S. Murphy, D. E. Gómez, P. Mulvaney, *J. Phys. Chem. C* **2018**, *122*, 13407.

[75] H. Huang, B. Chen, Z. Wang, T. F. Hung, A. S. Susha, H. Zhong, A. L. Rogach, *Chem. Sci.* **2016**, *7*, 5699.

[76] N. Aristidou, C. Eames, I. Sanchez-Molina, X. Bu, J. Kosco, M. S. Islam, S. A. Haque, *Nat. Commun* **2017**, *8*, 15218.

[77] A. M. A. Leguy, Y. Hu, M. Campoy-Quiles, M. I. Alonso, O. J. Weber, P. Azarhoosh, M. van Schilfgaarde, M. T. Weller, T. Bein, J. Nelson, P. Docampo, P. R. F. Barnes, *Chem. Mater.* **2015**, *27*, 3397.

[78] T. Moot, D. R. Dikova, A. Hazarika, T. H. Schloemer, S. N. Habisreutinger, N. Leick, S. P. Dunfield, B. A. Rosales, S. P. Harvey, J. R. Pfeilsticker, G. Teeter, L. M. Wheeler, B. W. Larson, J. M. Luther, *Chem. Mater.* **2020**, *32*, 7850.

[79] B. W. Boote, H. P. Andaraarachchi, B. A. Rosales, R. Blome-Fernández, F. Zhu, M. D. Reichert, K. Santra, J. Li, J. W. Petrich, J. Vela, E. A. Smith, *ChemPhysChem* **2019**, *20*, 2647.

[80] R. An, F. Zhang, X. Zou, Y. Tang, M. Liang, I. Oshchapovskyy, Y. Liu, A. Honarfar, Y. Zhong, C. Li, H. Geng, J. Chen, S. E. Canton, T. Pullerits, K. Zheng, *ACS Appl. Mater. Interfaces* **2018**, *10*, 39222.

[81] H. Wang, X. Zhang, N. Sui, Y. Hu, V. L. Colvin, X. Bai, Y. Zhang, A. L. Rogach, W. W. Yu, *J. Phys. Chem. Lett.* **2020**, *11*, 6168.

[82] M. I. Bodnarchuk, S. C. Boehme, S. ten Brinck, C. Bernasconi, Y. Shynkarenko, F. Krieg, R. Widmer, B. Aeschlimann, D. Günther, M. V. Kovalenko, I. Infante, *ACS Energy Lett.* **2019**, *4*, 63.

[83] J. Shi, F. Li, J. Yuan, X. Ling, S. Zhou, Y. Qian, W. Ma, *J. Mater. Chem. A* **2019**, *7*, 20936.

[84] C. Bi, X. Sun, X. Huang, S. Wang, J. Yuan, J. X. Wang, T. Pullerits, J. Tian, *Chem. Mater.* **2020**, *32*, 6105.

[85] L. Zhang, C. Kang, G. Zhang, Z. Pan, Z. Huang, S. Xu, H. Rao, H. Liu, S. Wu, X. Wu, X. Li, Z. Zhu, X. Zhong, A. K.-Y. Jen, *Adv. Funct. Mater.* **2021**, *31*, 2005930.

[86] K. Chen, Q. Zhong, W. Chen, B. Sang, Y. Wang, T. Yang, Y. Liu, Y. Zhang, H. Zhang, *Adv. Funct. Mater.* **2019**, *29*, 1900991.

[87] X. Zhang, H. Huang, Y. M. Maung, J. Yuan, W. Ma, *Chem. Commun.* **2021**, *57*, 7906.

[88] J. Khan, X. Zhang, J. Yuan, Y. Wang, G. Shi, R. Patterson, J. Shi, X. Ling, L. Hu, T. Wu, S. Dai, W. Ma, *ACS Energy Lett.* **2020**, *5*, 3322.

[89] E. Couderc, M. J. Greaney, R. L. Brutchey, S. E. Bradforth, *J. Am. Chem. Soc.* **2013**, *135*, 18418.

[90] Y. Xu, J. Yuan, S. Zhou, M. Seifrid, L. Ying, B. Li, F. Huang, G. C. Bazan, W. Ma, *Adv. Funct. Mater.* **2019**, *29*, 1806747.

[91] J. Yuan, X. Zhang, J. Sun, R. Patterson, H. Yao, D. Xue, Y. Wang, K. Ji, L. Hu, S. Huang, D. Chu, T. Wu, J. Hou, J. Yuan, *Adv. Funct. Mater.* **2021**, *31*, 2101272.

[92] R. Zhao, L. Xie, R. Zhuang, T. Wu, R. Zhao, L. Wang, L. Sun, Y. Hua, *ACS Energy Lett.* **2021**, *6*, 4209.

[93] A. Guerrero, J. You, C. Aranda, Y. S. Kang, G. Garcia-Belmonte, H. Zhou, J. Bisquert, Y. Yang, *ACS Nano* **2016**, 10, 218.

[94] K. Ji, J. Yuan, F. Li, Y. Shi, X. Ling, X. Zhang, Y. Zhang, H. Lu, J. Yuan, W. Ma, *J. Mater. Chem. A* **2020**, *8*, 8104.

[95] L. Hu, Q. Zhao, S. Huang, J. Zheng, X. Guan, R. Patterson, J. Kim, L. Shi, C.-H. Lin, Q. Lei, D. Chu, W. Tao, S. Cheong, R. D. Tilley, A. W. Y. Ho-Baillie, J. M. Luther, J. Yuan, T. Wu, *Nat. Commun.* **2021**, *12*, 466.

[96] A. Hazarika, Q. Zhao, E. A. Gaulding, J. A. Christians, B. Dou, A. R. Marshall, T. Moot, J. J. Berry, J. C. Johnson, J. M. Luther, ACS Nano **2018**, 12, 10327.

[97] M. Hao, Y. Bai, S. Zeiske, L. Ren, J. Liu, Y. Yuan, N. Zarrabi, N. Cheng, M. Ghasemi, P. Chen, M. Lyu, D. He, J.-H. Yun, Y. Du, Y. Wang, S. Ding, A. Armin, P. Meredith, G. Liu, H.-M. Cheng, L. Wang, Nat. Energy **2020**, 5, 79.

[98] F. Li, S. Zhou, J. Yuan, C. Qin, Y. Yang, J. Shi, X. Ling, Y. Li, W. Ma, ACS Energy Lett. **2019**, 4, 2571.

[99] S. Y. Park, H. C. Shim, ACS Appl. Mater. Interfaces **2020**, 12, 57124.

[100] J. Burschka, N. Pellet, S.-J. Moon, R. Humphry-Baker, P. Gao, M. K. Nazeeruddin, M. Grätzel, *Nature* **2013**, *499*, 316.

[101] M. Saliba, T. Matsui, J.-Y. Seo, K. Domanski, J.-P. Correa-Baena, M. K. Nazeeruddin, S. M. Zakeeruddin, W. Tress, A. Abate, A. Hagfeldt, M. Grätzel, *Energy Environ. Sci*. **2016**, *9*, 1989.

[102] A. Torres, L. G. C. Rego, *J. Phys. Chem. C* **2014**, *118*, 26947.

[103] H. J. Snaith, M. Grätzel, *Appl. Phys. Lett.* **2006**, *89*, 262114.

[104] J. H. Noh, N. J. Jeon, Y. C. Choi, Md. K. Nazeeruddin, M. Grätzel, S. I. Seok, *J. Mater. Chem. A* **2013**, *1*, 11842.

[105] T. H. Schloemer, J. A. Christians, J. M. Luther, A. Sellinger, *Chem. Sci.* **2019**, *10*, 1904.

[106] Y. Yue, N. Salim, Y. Wu, X. Yang, A. Islam, W. Chen, J. Liu, E. Bi, F. Xie, M. Cai, L. Han, *Adv. Mater.* **2016**, *28*, 10738.

[107] J. A. Dawson, A. J. Naylor, C. Eames, M. Roberts, W. Zhang, H. J. Snaith, P. G. Bruce, M. S. Islam, *ACS Energy Lett.* **2017**, *2*, 1818.

[108] H. Sarvari, X. Wang, Y. Wang, P. Zhang, S. Li, V. P. Singh, Z. Chen, *IEEE J. Photovolt.* **2018**, *8*, 1051.

[109] J. H. Heo, S. H. Im, J. H. Noh, T. N. Mandal, C.-S. Lim, J. A. Chang, Y. H. Lee, H. Kim, A. Sarkar, Md. K. Nazeeruddin, M. Grätzel, S. I. Seok, *Nat. Photonics* **2013**, *7*, 486.

[110] W. S. Yang, J. H. Noh, N. J. Jeon, Y. C. Kim, S. Ryu, J. Seo, S. I. Seok, *Science* **2015**, *348*, 1234.

[111] X. Ling, S. Zhou, J. Yuan, J. Shi, Y. Qian, B. W. Larson, Q. Zhao, C. Qin, F. Li, G. Shi, C. Stewart, J. Hu, X. Zhang, J. M. Luther, S. Duhm, W. Ma, *Adv. Energy Mater.* **2019**, *9*, 1900721.

[112] W. Yang, D. Zhong, M. Shi, S. Qu, H. Chen, *iScience* **2019**, *22*, 534.

[113] I. Mesquita, L. Andrade, A. Mendes, *ChemSusChem* **2019**, *12*, 2186.

[114] J. Yang, B. D. Siempelkamp, D. Liu, T. L. Kelly, *ACS Nano* **2015**, 9, 1955.

[115] S. N. Habisreutinger, T. Leijtens, G. E. Eperon, S. D. Stranks, R. J. Nicholas, H. J. Snaith, *Nano Lett.* **2014**, *14*, 5561.

[116] Q. Wang, Z. Lin, J. Su, Z. Hu, J. Chang, Y. Hao, *Nano Select* **2021**, *2*, 1055.

[117] K. Chen, W. Jin, Y. Zhang, T. Yang, P. Reiss, Q. Zhong, U. Bach, Q. Li, Y. Wang, H. Zhang, Q. Bao, Y. Liu, *J. Am. Chem. Soc*. **2020**, *142*, 3775.

[118] D. Jia, J. Chen, M. Yu, J. Liu, E. M. J. Johansson, A. Hagfeldt, X. Zhang, *Small.* **2020**, *16*, 2001772.

[119] M. M. Tavakoli, M. Nasilowski, J. Zhao, M. G. Bawendi, J. Kong, *Small Methods* **2019**, *3*, 1900449.

[120] L. Xiong, Y. Guo, J. Wen, H. Liu, G. Yang, P. Qin, G. Fang, *Adv. Funct. Mater.* **2018**, *28*, 1802757.

[121] Q. Jiang, X. Zhang, J. You, *Small* **2018**, *14*, 1801154.

[122] M. F. M. Noh, C. H. Teh, R. Daik, E. L. Lim, C. C. Yap, M. A. Ibrahim, N. A. Ludin, A. R. bin Mohd Yusoff, J. Jang, M. A. M. Teridi, *J. Mater. Chem. C* **2018**, *6*, 682.

[123] K. Nakata, A. Fujishima, *J. Photochem. Photobiol., C* **2012**, *13*, 169.

[124] C. Xiao, Q. Zhao, C.-S. Jiang, Y. Sun, M. M. Al-Jassim, S. U.Nanayakkara, J. M. Luther, *Nano Energy* **2020**, *78*, 105319.

[125] C. Ding, F. Liu, Y. Zhang, D. Hirotani, X. Rin, S. Hayase, T. Minemoto, T. Masuda, R. Wang, Q. Shen, *Nano Energy* **2020**, *67*, 104267.

[126] J. Chen, N.-G. Park, *J. Phys. Chem. C* **2017**, *122*, 14039.

[127] J. Chen, D. Jia, E. M. Johansson, A. Hagfeldt, X. Zhang, *Energy Environ. Sci.* **2021**, *14*, 224.

[128] J. Lian, B. Lu, F. Niu, P. Zeng, X. Zhan, *Small Methods* **2018**, *2*, 1800082.

[129] S. B. Shivarudraiah, M. Ng, C.-H. A. Li, J. E. Halpert, *ACS Appl. Energy Mater.* **2020**, *3*, 5620.

[130] X. Huang, J. Hu, C. Bi, J. Yuan, Y. Lu, M. Sui, J.Tian, *Chem. Eng. J.* **2021**, *421*, 127822.

[131] J. Kim, B. Koo, W. H. Kim, J. Choi, C. Choi, S. J. Lim, J.-S. Lee, D.-H. Kim, M. J. Ko, Y. Kim, *Nano Energy* **2019**, *66,* 104130.

[132] X. Zhang, H. Huang, X. Ling, J. Sun, X. Jiang, Y. Wang, D. Xue, L. Huang, L. Chi, J. Yuan, W. Ma, *Adv. Mater.* **2021**, *34*, 2105977.

[133] A. Kojima, K. Teshima, Y. Shirai, T. Miyasaka, *J. Am. Chem. Soc.* **2009**, *131*, 6050.

[134] W. Ke, G. Fang, Q. Liu, L. Xiong, P. Qin, H. Tao, J. Wang, H. Lei, B. Li, J. Wan, *J. Am. Chem. Soc.* **2015**, *137*, 6730.

[135] A. Bera, A. D. Sheikh, M. A. Haque, R. Bose, E. Alarousu, O. F. Mohammed, T. Wu, *ACS Appl. Mater. Interfaces* **2015**, *7*, 28404.

[136] A. Garcia, G. C. Welch, E. L. Ratcliff, D. S. Ginley, G. C. Bazan, D. C. Olson, *Adv. Mater.* **2012**, *24*, 5368.

[137] J. Ma, Z. Lin, X. Guo, J. He, Z. Hu, J. Su, J. Zhang, J. Chang, Y. Hao *Mater. Today Energy* **2019**, *14*, 100351.

[138] E. H. Anaraki, A. Kermanpur, L. Steier, K. Domanski, T. Matsui, W. Tress, M. Saliba, A. Abate, M. Grätzel, A. Hagfeldt, J.-P. Correa-Baena, *Energy Environ. Sci.* **2016**, *9*, 3128.

[139] V. Rohnacher, F. Ullrich, H. Eggers, F. Schackmar, S. Hell, A. Salazar, C. Huck, G. Hernandez-Sosa, U. W. Paetzold, W. jaegermann, A. Pucci, *Adv. Mater. Technol.* **2021**, *6*, 2000282.

[140] J. A. Raiford, S. T. Oyakhire, S. F. Bent, *Energy Environ. Sci.* **2020**, *13*, 1997.

[141] Z. Xing, J. Xiao, T. Hu, X. Meng, D. Li, X. Hu, Y. Chen, *Small Methods* **2020**, *4*, 2000588.

[142] Y. Lee, S. Lee, G. Seo, S. Paek, K. T. Cho, A. J. Huckaba, M. Calizzi, D.-W. Choi, J.-S. Park, D. Lee, H. J. Lee, A. M. Asiri, M. K. Nazeeruddin, *Adv. Sci.* **2018**, *5*, 1800130.

[143] J. Kruszyńska, J. Ostapko, V. Ozkaya, B. Surucu, O. Szawcow, K. Nikiforow, M. Hołdyński, M. M. Tavakoli, P. Yadav, M. Kot, G. P. Kołodziej, M. Wlazło, S. Satapathi, S. Akin, D. Prochowicz, *Adv. Mater. Interfaces* **2022**, 2200575.

[144] H. -S. Yun, K. Noh, J. Kim, S. H. Noh, G. -H. Kim, W. Lee, H. B. Na, T. -S. Yoon, J. Jang, Y. Kim, S. -Y. Cho, *Phys. Status Solidi RRL.* **2020**, *14*, 1900573.

[145] B. Tang, X. Zhao, L. J. Ruan, C. Qin, A. Shu, Y. Ma, *Nanoscale* **2021**, *13*, 10600.

[146] X. Zhang, M. Lu, Y. Zhang, H. Wu, X. Shen, W. Zhang, W. Zheng, V. L. Colvin, W. W. Yu, *ACS Cent. Sci.* **2018**, *4*, 10, 1352.

[147] Y. Liu, Y. Dong, T. Zhu, D. Ma, A. Proppe, B. Chen, C. Zheng, Y. Hou, S. Lee, B. Sun, E. H. Jung, F. Yuan, Y.-k. Wang, L. K. Sagar, S. Hoogland, F. P. G. de Arquer, M.-J. Choi, K. Singh, S. O. Kelley, O. Voznyy, Z.-H. Lu, E. H. Sargent, *J. Am. Chem. Soc.* **2021**, *143*, 15606.

[148] G. H. Carey, K. W. Chou, B. Yan, A. R. Kirmani, A. Amassian, E. H. Sargent, *MRS Commun.* **2013**, *3*, 83.

[149] H. Aqoma, M. A. Mubarok, W. T. Hadmojo, E.-H. Lee, T.-W. Kim, T. K. Ahn, S.-H. Oh, S.-Y. Jang, *Adv. Mater.* **2017**, *29*, 1605756.

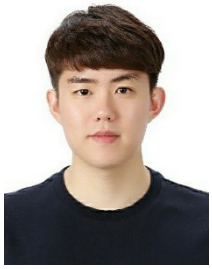

Seyeong Lim received his B.S. degree from Department of Materials Science and Engineering, POSTECH in 2017. He has been a Ph.D. candidate student under the supervision of Prof. Taiho Park at Department of Chemical Engineering in POSTECH. He participated in an international student research program at RIKEN CEMS, Japan from June to September 2019. His research interests are synthesis, purification and surface engineering of lead halide perovskite quantum dots for optoelectronic devices.

Sanghun Han received his B.S. degree from Department of Materials Science and Engineering, Hongik University in 2020. He has been an integrated M.S.&Ph.D. candidate student under the supervision of Prof. Jongmin Choi at the Department of Energy Science and Engineering at DGIST. His research interests are synthesis and surface modification of lead halide perovskite quantum dots for optoelectronic applications.

Jongmin Choi is an Assistant Professor in the Department of Energy Science & Engineering at DGIST. He received his B.S and Ph.D. degree in department of Chemical Engineering at POSTECH in 2010 and 2016, respectively, under the supervision of Prof. Taiho Park. After that, he carried out his postdoctoral research in Edward H. Sargent research group at University of Toronto, Canada from 2016 to 2018. His research interests include the development of next generation energy materials for optoelectronic devices.

Taiho Park is a Namko endowed chair professor of POSTECH. He received his Ph.D degree from the University of Cambridge, UK, under the supervision of Prof. Andrew B. Holmes in 2003, and then worked as a research fellow with Prof. Steven C. Zimmerman at the University of Illinois (Urbana-Champaign), USA. He has joined the faculty in the Department of Chemical Engineering at POSTECH in 2007. Currently, he has served as a member of the Editorial Advisory

Board of Advanced Energy Materials since 2022. His current research interests include the material properties and device functions of optoelectronic devices.

The table of contents entry

This review intensively discusses the stability issues and their overcome strategies in $CsPbI_3$ perovskite quantum dot solar (PQD) cells. The detailed degradation mechanisms of $CsPbI_3$ PQDs are provided from the material and device architectural viewpoints. Furthermore, related design strategies for stable $CsPbI_3$ PQD solar cells along with possible future perspectives are proposed.

Seyeong Lim,[‡] Sanghun Han,[‡], Dohyun Kim, Jihyun Min, Jongmin Choi and Taiho Park**

Key factors affecting the stability of $CsPbI_3$ perovskite quantum dot solar cells: a comprehensive review